A STUDY OF TWO DIMENSIONAL NMR USING THE SUPERSPIN FORMALISM

A STUDY OF TWO DIMENSIONAL NMR USING THE SUPERSPIN FORMALISM

By

IAN BURTON, B.Sc.

A Thesis

Submitted to the School of Graduate Studies

in Partial Fulfilment of the Requirements

for the Degree

Master of Science

McMaster University

Master of Science (1993)	**McMaster University**
(Chemistry)	Hamilton, Ontario
TITLE:	A Study of Two Dimensional NMR Using the Superspin Formalism
AUTHOR:	Ian Burton, B.Sc. (McMaster)
SUPERVISOR:	Professor A.D. Bain
NUMBER OF PAGES:	viii, 86

ABSTRACT

Two-dimensional C-H chemical shift correlation spectroscopy provides a large amount of information in a two dimensional matrix. Many variations of these experiments have been in an effort to enhance the information content of these experiments. Decoupling of multiplet signals is one method used to increase the sensitivity of an NMR experiment. Simple broadband decoupling in ω_2 is done by irradiating the correlated channel during acquisition. Decoupling in ω_1 must be done using less direct methods, one of which is to use bilinear rotation decoupling. The traditional description of the effect that a BIRD pulse has on the spin systems is based on a simple AX system which is at equilibrium at the beginning of the pulse, which does not apply in many real systems.

This study uses the Superspin formalism to show in more detail the behaviour of more complex spin systems during the BIRD sequence, and the effect of varying parameters within the BIRD sequence. This treatment involved the derivation of complete spherical tensor descriptions of AX, AX_2, and AX_3 spin systems. This allowed the derivation of a mathematical description of an INEPT style pulse sequence, where the refocussing pulse in INEPT was replaced with the BIRD sequence. The derivation of the general evolution transformations of the spherical tensors in Liouville space also allowed the theoretical treatment to be done in a single basis, where earlier implementations of the Superspin formalism converted between a spherical tensor basis for the treatment of pulses and a Hamiltonian basis for the treatment of delays. This theoretical treatment allows the derivation of a functional form for the dependence of the carbon signal intensity on the variation of the interpulse delay in the BIRD sequence.

This formalism was also used to analyze the occurrence of artifacts in two dimensional heteronuclear shift correlation spectra, due to strong coupling between methylene protons. These artifacts were studied in experiments that attempt broadband homonuclear decoupling in ω_1 through the use of constant evolution time between the initial excitation pulse and polarization transfer. Two experiments were analyzed, the COLOC experiment and the HETRES experiment. The superspin formalism was used to deduce a functional form for the intensity of the artifact as a function of the strength of the coupling between the methylene protons.

Acknowledgements

I would like to extend my sincerest appreciation to my supervisor, Dr. Alex D. Bain, for his patience, support and encouragement over the years that I had the privilege to work with him. I would also like to thank the people in Dr. Bain's research group who I have shared many enjoyable experiences with; most notably Ms. Janice Cramer, Mr. Gregory Duns, Dr. D. Bruce Fulton, Mr. Stephen Hughes, Dr. Traci Bryar and Ms. Lydia Lao. I would also like to thank Prof. William Reynolds of the University of Toronto for his help and discussion. Mr. Brian Sayer and Dr. Donald Hughes for their support and assistance and from whom I have learned a great deal, and Dr. Thomas Slee who has given me encouragement through this last year. I would also like to thank my parents and my family who have never failed to support me throughout my university career.

Finally, I would like to express my deepest appreciation to my wife, Erica, who through her patience and support has been there for me through it all, and it is to her that I dedicate this work.

Table of Contents

List of Figures

List of Tables

Chapter 1

Introduction

The area of high resolution NMR spectroscopy has undergone tremendous growth since the introduction of pulse Fourier transform spectrometers in the 1960's. The advent of pulse techniques to NMR has led to the development of hundreds of different experiments designed to enhance signal to noise or to modify the information content of the NMR spectrum. Today NMR spectroscopy has become a routine research tool and has permeated almost every branch of chemistry including biochemistry, organic, inorganic and solid state chemistry, geochemistry, polymer engineering, and medicine. [1-6]

In 1945, NMR effects were first observed in bulk media independently by Purcell, Torrey and Pound [7] and Bloch, Hansen and Packard.[8] This was an observation of a hypothesis put forth by Pauli in the early 1920's that stated that some atomic nuclei should possess magnetic moments.[9] In an external magnetic field, these magnetic moments will experience a torque and will precess about the applied magnetic field. The application of an oscillating magnetic field, applied at right angles to the static magnetic field and oscillating at the radio frequency corresponding to the precession frequency of the nucleus, will cause an absorption of energy by the nucleus.

The nucleus can be a very sensitive probe of the local magnetic field experienced by the nucleus in a molecular system. Thus the NMR spectrum, if acquired with sufficient resolution, can yield information about nuclear magnetic effects from other nuclei in the same molecule (spin-spin coupling; nuclear Overhauser effect), in other molecules (spin-lattice relaxation; spin diffusion), and the shielding effects of bonding electrons at the nucleus and π-bonding electrons (chemical shift). All of these observations can be correlated to molecular connectivity and structure. The high sensitivity of the nucleus to all these effects makes NMR an invaluable tool for researchers studying molecular structure and environmental effects such as molecular dynamics [10-12] and solvent-solute interactions. [13-15]

In high resolution NMR, the most common information gained from the spectrum is chemical connectivity through the chemical shift and splitting patterns of the NMR signals. Scalar spin-spin coupling will split the signals into multiplets, and the multiplicity, line spacing and intensities within the multiplets gives information about molecular connectivity and conformation.[16-18] A great deal of attention has been devoted to the extraction of NMR parameters from the appearance of complex spin systems and the correlation of these parameters to structural constraints. In this respect NMR can give complementary information to x-ray crystallography, particularly in complex biological systems where the structure in solution may be quite different than in the crystalline phase, or in systems where it is difficult to obtain crystals.

In addition to correlating the NMR spectrum to a framework through the analysis of multiplet patterns, NMR can give information about the conformation of a molecule

through the nuclear Overhauser effect. Relaxation pathways via dipolar coupling can effect NMR signal intensities. These changes in intensity can be investigated by perturbing one of the coupled signals, and distance information can be obtained from these intensities. This can then be used to determine conformational constraints in large molecules when an nOe is observed between nuclei in the same molecule. This has been used effectively in the study of the conformation of biological systems. [19,20]

In complex molecules, there may be many signals which have complex splitting patterns, and that overlap in a narrow region in the spectrum. This problem has been overcome in many cases by the development of more powerful magnets. With increasing magnetic field the chemical shift difference (in Hz) of overlapping signals will increase, while the spacing within a multiplet will remain constant. This will make the spectrum easier to interpret because of less overlap, the multiplet patterns will become slightly simpler, and the sensitivity will increase, as the population difference between energy levels will increase with increasing field strength. There are always cases however, where increasing the field strength does not adequately resolve overlapped multiplets. Because of cases like this, NMR spectroscopy has been expanded into a second dimension and beyond through correlation spectroscopy. [21,22]

Sensitivity of the NMR experiment has also been enhanced through the use of signal averaging, particularly with pulse techniques. Signal averaging increases the signal to noise ratio of the spectrum by a factor of $n^{1/2}$, n being the number of transients making up the average. This averaging can be done using scanned (continuous wave) spectra, however it is more efficiently applied to pulse NMR, where the signal averaging is done

in the time domain and the resulting time domain spectrum (or free induction decay or FID) is Fourier transformed to yield the frequency domain spectrum. This has not only made it possible to acquire spectra of dilute solutions or of small amounts of compound, but to acquire spectra of nuclei that have lower sensitivity than protons, as well as using pulse techniques to manipulate the spin systems to gain additional information, or to modify the information content of the spectrum.

Pulse Fourier transform NMR has led to the development of a library of hundreds of NMR experiments.[23] Pulse experiments such as INEPT or DEPT increase the sensitivity of spectra involving insensitive nuclei such as ^{13}C through polarization transfer from a more sensitive nucleus via spin-spin coupling. These same experiments allow spectral editing, where methyl, methylene, methine and quaternary carbons can be distinguished. In a similar experiment, J-spectroscopy, signals can be identified through multiplicity sorting. This has ultimately led to multidimensional NMR and correlation spectroscopy where signals in one dimension are correlated to signals in another dimension through cross peaks. Two dimensional NMR was first suggested by Jeener in 1971 [24], and the first experiment published was by Aue, Bartholdi and Ernst in the mid 1970's.[25,26] Examples of two dimensional experiments include two dimensional J-spectroscopy where one dimension represents chemical shift in Hz and the second dimension represents coupling constants in Hz. This is commonly represented by multiplet patterns in one dimension separated by the chemical shift of the nucleus. Another more popular type of two dimensional spectroscopy is chemical shift correlation spectroscopy where the chemical shift of one nucleus is correlated to the chemical shift

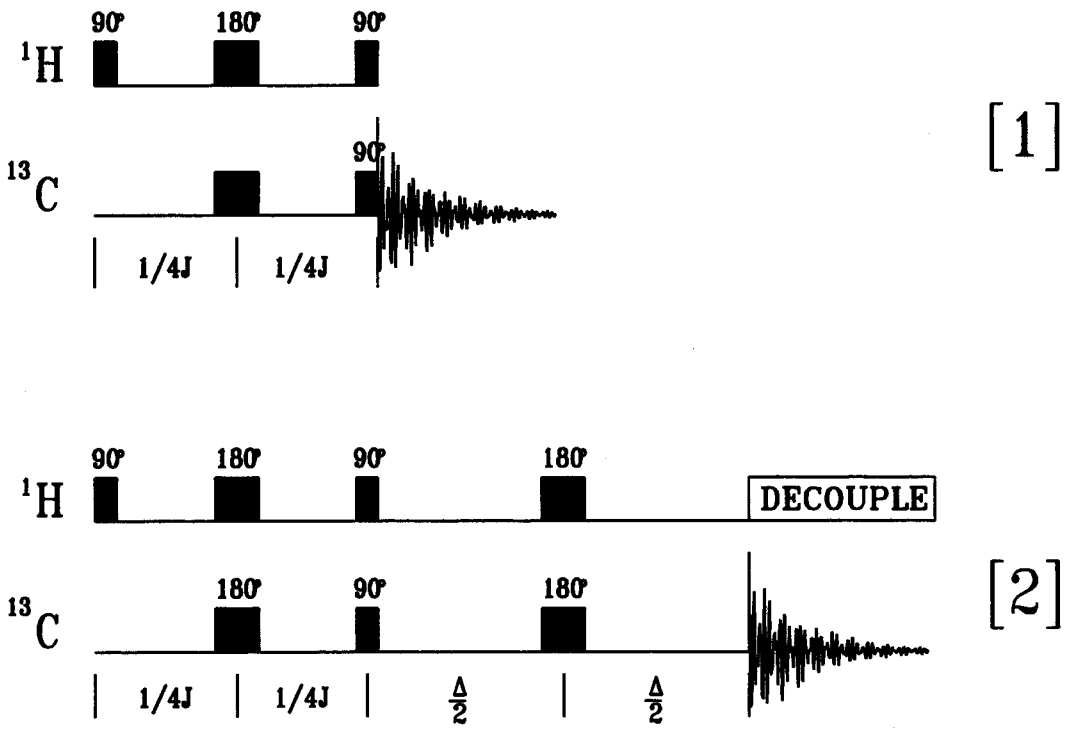

Figure 1.1: Pulse sequences for standard INEPT [1] and refocussed INEPT [2].

of another related to it through scalar coupling. This can be done between nuclei of the same type as in the homonuclear COSY experiment [27] or between different nuclei, as in the heteronuclear shift correlation experiment or FUCOUP [28,29]. There is also a two dimensional experiment which shows correlations between nuclei which are in chemical exchange [30] or show nuclear Overhauser enhancement.[31]

All two dimensional NMR experiments are acquired as a series of free induction decays, with some experimental parameter, usually a delay, incremented in a regular fashion between each acquisition. In the homonuclear COSY experiment, the initial 90° pulse creates xy magnetization, and then these are allowed to evolve for a time t_1. A second 90° pulse is applied to the system which causes frequencies from other transitions

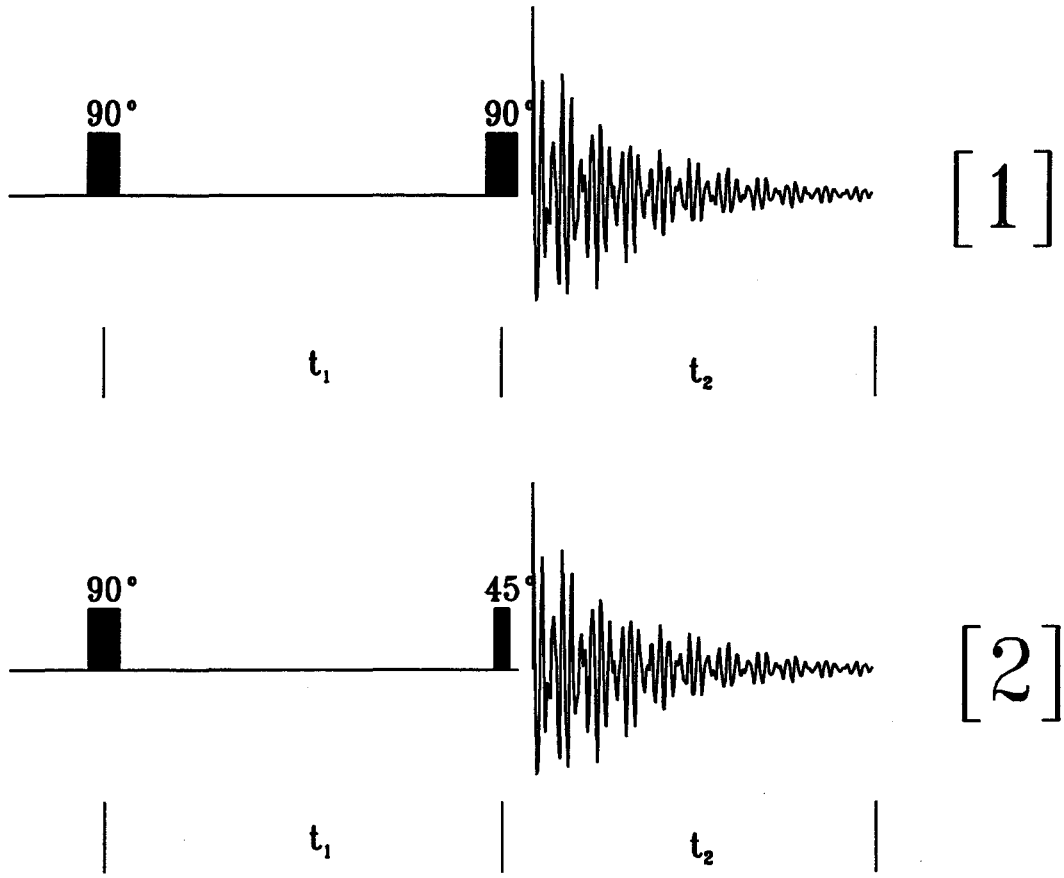

Figure 1.2: Pulse sequences for normal COSY [1] and COSY-45 [2].

in the spin system to modulate transitions which have evolved over t_1. The resulting data matrix is Fourier transformed first with respect to t_2 to give a series of spectra with lines modulated by the frequencies of coupled transitions. A second Fourier transform with respect to t_1 then yields the cross peaks correlating signals in f_1 with signals in f_2. This transformed data matrix contains peaks which correlate signals in one dimension with signals in the second dimension. The cross peaks in the COSY experiment will show all correlations through all of the couplings resulting in complex cross peaks, and lines within a multiplet will show correlations to each other very close to the diagonal, giving a very

cluttered looking spectrum around the diagonal. A variation of this experiment, known as COSY-45, simplifies these cross peaks and reduces the correlations within multiplets around the diagonal portion of the spectrum. This makes it simpler to identify correlations between signal in a region of overlapped multiplets.

In the same way that homonuclear two dimensional NMR can be used to help determine connectivity and multiplicity in spectra of complex molecules where many signals overlap, heteronuclear two dimensional NMR makes it possible to correlate signals between dissimilar nuclei. The most common example of this is the correlation of ^{13}C signals with ^{1}H signals in organic compounds. This experiment was described by Maudsley and Ernst in 1977[32], and was performed by detecting the carbon spectrum indirectly through the interferogram produced by coupled protons, analogous to the acquisition of correlation signals in the homonuclear experiment. This is known today as inverse detection and the more common approach today is to detect the carbon spectrum directly using a modification of the INEPT experiment.[33]

The INEPT style experiment modulates the transfer of polarization from protons to carbons with respect to t_1, and the Fourier transform in this dimension will yield cross peaks that correspond to the frequencies of proton signals that are coupled to those carbons. This is similar to the INEPT experiment without refocussing and decoupling in that it shows all couplings in the spin systems. Decoupling in ω_2 can be achieved in the same manner as in the refocussed INEPT experiment; a refocussing delay is needed to bring the multiplet components of the detected nucleus approximately back in phase so that broadband decoupling can be applied during acquisition. Thus a delay, Δ_2 is

introduced into the experiment after polarization transfer. Heteronuclear decoupling in ω_1 is achieved by placing a 180° pulse at the midpoint of the evolution time t_1. This will refocus the heteronuclear coupled vectors at the end of the t_1 delay. In order to transfer polarization to the carbons however, the multiplets must be allowed to dephase, thus a delay Δ_1 is inserted between the end of t_1 and polarization transfer.

Resolution can be further enhanced in ω_1 if the homonuclear multiplet patterns in ω_1 can be collapsed [34]. This is done by applying a pulse which selectively inverts proton coherences arising from protons attached to ^{13}C but leaves those attached to ^{12}C unchanged. If this pulse is placed at the centre of the evolution time t_1 the effect will be to refocus multiplets due to vicinal protons. Since the natural abundance of ^{13}C is very small (~1.1%) the vicinal protons will be mostly bonded to ^{12}C. A pulse sequence which satisfies this requirement is known as a Bilinear Rotation Operator, or BIRD pulse [35]. This pulse sandwich is made up of 90°(H)-τ-180°(H,C)-τ-90°(H) pulses, where the delay τ is equal to $1/(2*{}^1J_{CH})$. This strategy works well providing the homonuclear coupling is much smaller than $^1J_{CH}$, and there is not a large variation in $^1J_{CH}$. In addition, geminal protons will not be decoupled as they are both attached to a ^{13}C.

In the INEPT based HSC experiment, the delays Δ_1 and Δ_2 are generally chosen so that polarization was transferred from directly bonded protons. In order to optimize the correlations between ^{13}C and long range coupled protons, these delays must be optimized for the long range coupling constants, where long range implies $^nJ_{CH}$ with n>1. Problems can arise with this optimization of the delays, in that to afford optimum polarization transfer from the long range protons, the defocussing delay, Δ_1, is long

enough so that direct bonded magnetizations may orient in a fashion that will transfer magnetization from the directly bonded protons, or to destructively interfere with the long range magnetizations resulting in no net polarization transfer. This can cause problems in that the delays may be optimized for different long range couplings and these different settings may cause the direct bond couplings to be either in or out of phase. This will result in some long range correlations being attenuated or some direct correlations having a large intensity. Also, the long range coupling constants have a broader range relative to the short range coupling constants making it harder to optimize the refocussing delays. This may cause correlations to drop out in some systems. There have been many attempts to enhance the long range HSC experiment either through the elimination of direct bond correlations or through the elimination of homonuclear coupling. A series of these experiments come under the classification of constant evolution time experiments, as the second dimension is acquired by incrementing a mixing pulse through a constant time period between initial excitation and polarization transfer.

One early example of the constant time experiments is COLOC.[36] In this sequence simultaneous 180° pulses are incremented through a constant evolution period, *T*, between the initial proton 90° pulse and polarization transfer. The constant evolution time provides broadband homonuclear decoupling in f_1, since the magnetizations due to homonuclear coupling are not modulated with respect to t_1. Polarization transfer is maximized by setting the constant time to $1/(2*J_{CH})$. Since the experiment evolves over a constant time, the interferogram in t_1 will not be attenuated by relaxation and thus will show no exponential decay. This can be a drawback in that in order to perform any zero

filling in t_1 it is necessary to apply heavy apodization in order to minimize truncation artifacts. Another drawback is that the resolution in f_1 will be limited because of the constant evolution time. Any effort to increase the resolution by increasing the number of points acquired will simply increase the spectral width in f_1, and resolution will remain constant. This can be alleviated to a certain degree by increasing the value of *T* to larger odd multiples of $1/(2*J_{CH})$. However, since there is a longer time between initial excitation and acquisition, the intensity of the signal will be attenuated with respect to that done with shorter values of T.

CHAPTER 2

Theory

Many nuclei have a property known as spin which is the quantum mechanical analogue of a classical spinning top. This gives the nucleus spin angular momentum, and since the nucleus has charge, it will also have a quantized magnetic moment. The spin is given the quantum number I and the magnetic quantum number is m. The number of m levels is related to the spin quantum number through the relationship:

$$\mathbf{m = 2I + 1} \qquad \textbf{[2.1]}$$

and the magnetic quantum numbers have values in the range m = { -I, -I+1, ... I-1, I }. The magnetic moment, μ, is always parallel to the angular momentum. The magnetic properties of a nucleus are usually expressed in terms of the ratio of the magnetic moment and the total angular momentum. This ratio is known as the magnetogyric ratio, γ:

$$\gamma = \frac{2\pi\mu}{Ih} \qquad \textbf{[3.2]}$$

Thus for protons and ^{13}C nuclei which have I = 1/2, there exists two degenerate magnetic quantum numbers, m = $\pm$ 1/2. This degeneracy can be lifted by placing the nucleus in a uniform magnetic field, B_0, causing the levels to split proportionately to the strength of the magnetic field. The energy difference between the m = +1/2 and m = -1/2 is proportional to the strength of the magnetic field:

$$\Delta E = h\nu_0 = \frac{\mu B_0}{I} \qquad [2.3]$$

When the magnetic field is applied, the nucleus does not merely align its magnetic moment with the applied magnetic field, but since the nucleus is spinning (i.e. it has quantized spin) it also has spin angular momentum and the nucleus will experience a torque and the spin axis will precess about the direction of the applied magnetic field. The precession frequency is known as the Larmor frequency, and is equivalent to the frequency associated with the difference in energy of the magnetic spin levels in the magnetic field:

$$\omega_0 = \gamma B_0 = \frac{2\pi\mu B_0}{hI} \qquad [2.4]$$

Thus increasing the strength of the magnetic field does not increase the amount that the spin will align with B_0, but will merely increase the Larmor frequency and the energy difference between the spin levels. The nucleus can be made to flip the direction of its spin axis to the opposite direction by the application of a second magnetic field, B_1 at right angles to B_0 and oscillating at the Larmor frequency.

The separation of the energy levels, ΔE, can be seen to be $2\pi\mu B_0$ for a spin 1/2. If the B_1 field is rotated at a frequency approaching the Larmor frequency, a resonance effect will be observed as the Larmor frequency is passed. This is the case in CW NMR, with the spectrum detected as the absorption of energy from the rf field or through an induced voltage created by the flipping of the magnetic dipoles at resonance.

The description of pulse NMR is aided by the use of a frame of reference which

rotates at the Larmor frequency. In this frame of reference the magnetizations which precess about the z axis are static with respect to the z′ axis in the rotating frame. The individual magnetizations from each nucleus contribute to a net equilibrium in a canonical ensemble of nuclei. This net magnetization is aligned along the z′ axis when the system is at equilibrium, and it is the motion of this vector which is followed in the rotating frame during the course of a pulse sequence. Another simplification that results from the adoption of a rotating frame of reference is that if a second magnetic field, B_1, oscillating at the Larmor frequency, is applied to the system at right angles to B_0, this new magnetic field can be represented as a stationary vector in the rotating frame. (Figure 2.1) The phase of the B_1 field with respect to the Larmor frequency is represented by the direction of the vector in the x′y′ plane.

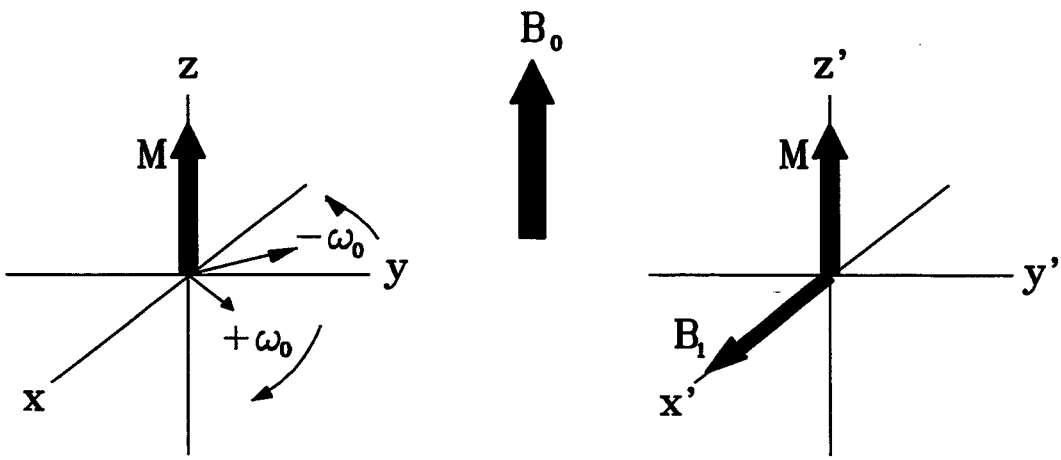

Figure 2.1: Comparison of the laboratory frame (left) and the rotating frame (right).

In the rotating frame then, the pulse is the application of a second static magnetic field, B_1, at right angles to the external field B_0. An important assumption with regards to a pulse is that the B_1 field dominates all other interactions during a pulse. A result of

this assumption is that during a pulse, the net magnetization will precess about the magnetic field B_1. This also means that all other effects, such as relaxation and spin - spin coupling are ignored for the duration of a pulse.

The most common method of observing NMR signals in modern spectrometers is by the use of pulse methods to create a time domain signal and subsequent Fourier transformation to create the frequency domain spectrum. The pulse of rf energy has an effective bandwidth which is inversely proportional to the width of the pulse, and is broad enough to cover the spectral range of proton and carbon spectra in solution. Since the B_1 field strength is much larger in the pulse experiment than in the CW experiment, the net magnetization, M_0, will precess about B_1 for the duration of the pulse. The angle α which the magnetization precesses from its equilibrium position defines the duration of the pulse, and is related to the strength of the perturbing field B_1 through the relationship:

$$\alpha = \gamma B_1 t_p \qquad [2.5]$$

In order to observe maximum signal intensity, a pulse angle of 90° is used.

After the application of a 90° pulse the net magnetization is aligned in the x′y′ plane, where it begins to precess about the B_0 (z′) axis. The spins then begin to relax in the x′y′ plane due to spin-spin relaxation, and increase in the z′ plane due to spin lattice relaxation. This oscillation and loss of phase coherence in the x′y′ plane is detected as a free induction decay (FID) and is Fourier transformed to give the frequency domain spectrum.

The superspin formalism for pulse NMR [37-42] is a density matrix formalism which has as its elements, operators on eigenstates which represent transitions between those

eigenstates. The density matrix represents the set of all physically observable quantities associated with a spin system. This set of observables is presented as a vector in operator space (or Liouville space). The effects of pulses and delays on a spin system is easily represented as transformations on the density matrix (this is the more reasonable basis to work in since the pulse acts on transitions between eigenstates rather than the eigenstates themselves). Thus the effect of a pulse is represented by the multiplication of the density 'vector' by a transformation matrix to give another vector. The angular momentum character of the superspin tensors in Liouville space represent the coupled angular momentum of the eigenstates that contribute to the transition represented by the superspin tensors. Thus the density matrix elements can be represented by quantum numbers representing the total angular momentum of a transition and the z component of the angular momentum, or magnetic quantum number. It is then possible to describe the effect of a pulse on a transition between eigenstates as a transformation of the angular momentum properties associated with the transition in analogy to the transformation under rotation of angular momentum eigenstates. The rotation is represented by the set of rotation matrices known as the Wigner rotation matrices, and the effect of a pulse on the density matrix is simply a multiplication by the appropriate Wigner matrices.[43]

The development of the description of NMR transitions using superspin was first introduced by Banwell and Primas [44] as the 'direct method' for calculating NMR spectra. In this description a superoperator was derived which has as its eigenvalues, the frequencies representing the transitions between spin eigenstates. The set of superoperators for a given spin system is a vector in Liouville space, which is a Euclidean

space representing all of the operators in spin space. In spin space the concept of transverse magnetization is associated with transitions between eigenstates $|\mathbf{r}\rangle \rightarrow |\mathbf{s}\rangle$ where $M_r - M_s = \pm 1$. In the more general case, where $\Delta M \geq \pm 1$, in spin space this is represented by non-vanishing off diagonal elements of the density matrix, σ_{rs}, representing a coherent superposition between eigenstates $|\mathbf{r}\rangle$ and $|\mathbf{s}\rangle$. This coherent superposition occurs only between pairs of eigenstates, and the difference in magnetic quantum number, ΔM_{rs}, is referred to as the order of coherence or the coherence level. Thus $\Delta M = 0$ represents zero quantum coherence, $\Delta M = 1$ single quantum coherence, up to $\Delta M = p$ for p-quantum coherence. The number of coherence levels will be limited by the number of spins in the system. In Liouville space the density matrix is made up of operators representing these coherent superpositions and the elements of the density matrix are written in a form which describes the angular momentum character of the transitions:

$$|\mathbf{M_K})$$

where M is the quantum number representing the superspin or the total angular momentum of the transition, and K is the z component of the angular momentum, or the coherence level.

In complex spin systems, there is a unitary transformation between the differences between the energy levels in Hilbert space and the linear operators in Liouville space.[45] Thus the density matrix representation of the spin system in terms of spherical tensors can be derived from the eigenstates of the system. Once this has been done, however, these eigenstates need not be used again. In earlier applications and descriptions of the superspin formalism, [38-42] the effect of a pulse on the density matrix was determined in

the spherical tensor basis and then a unitary transformation was derived to transform the density matrix back to the Hamiltonian basis. The effects of the delay was determined in this basis. In this study, however, equations for the general evolution as spherical tensors in Liouville space were derived so that the effect of a delay on the density matrix can be determined in without transforming to the Hamiltonian basis. In complex spin systems, the density matrix may be represented by spherical tensors which represent coupled spin systems rather than products of individual spin tensors. There exists a unitary transformation between the coupled and uncoupled representations, which follows the same rules as coupling of angular momenta.

The preliminary work in this study involved determining the representations of the fully coupled spherical tensors in terms of the uncoupled representation, for the AX, AX_2, and AX_3 spin systems. The general evolution formulae were then derived for the spherical tensor basis for these spin systems. In this application of the superspin formalism, an entire NMR experiment can be followed through mathematically while remaining in the same basis.

The transitions that make up the density matrix can be found by solving the eigenvalues for the Liouville equation directly, in this case:[45]

$$\frac{\partial \rho}{\partial t} = -iL\rho - R(\rho - \rho_{eq}) \qquad [2.6]$$

with eigenvectors $|\phi_1\rangle\langle\phi_2|$, and eigenvalues $\varepsilon_1 - \varepsilon_2$. In this case the state functions for the Hamiltonian basis are known, and vectors of the form $|\phi_1\rangle\langle\phi_2|$ can be constructed from this basis. The spherical tensors in Liouville space can be related to the more familiar spin space operators in the single spin case.[37]

$$|0) = (\frac{1}{\sqrt{2}})\hat{1} = \frac{1}{\sqrt{2}}\{|\alpha\rangle\langle\alpha| + |\beta\rangle\langle\beta|\} \quad [2.7]$$

$$|1_{+1}) = -(\hat{I}_x + i\hat{I}_y) = -|\alpha\rangle\langle\beta| \quad [2.8]$$

$$|1_0) = (\frac{1}{\sqrt{2}})\hat{I}_z = \frac{1}{\sqrt{2}}\{|\alpha\rangle\langle\alpha| - |\beta\rangle\langle\beta|\} \quad [2.9]$$

$$|1_{-1}) = (\hat{I}_x - i\hat{I}_y) = |\beta\rangle\langle\alpha| \quad [2.10]$$

Since the single spin density matrix elements are spherical tensors, they can be combined in the same way as angular momentum operators, to form spherical tensors representing the transitions associated with coupled spin systems. These spherical tensors have a notation similar to the single spin case:

$$|\mathbf{M^S_s,k})$$

where M is the rank of the spherical tensor,

s is the subscript or z component of the angular momentum,

S is the symmetry with respect to the coupled spins,

k represents the number of rank 1 single spin spherical tensors.

The creation of a coupled basis set proceeds through the following steps:

1. Identification of the energy levels of the coupled spin system through the eigenvalues of the Hamiltonian basis, and identification of the spin space transitions between pairs of these eigenstates. All multiple quantum transitions are identified.

2. The transitions are expressed in terms of the spin space eigenvectors and the

differences between the spin space eigenvalues.

3. The above expressions relating the spin space operators to the single spin spherical tensors are used to express the transitions in terms of combinations of single spin spherical tensors.

4. The rules for coupling angular momenta are used to combine single spin spherical tensors to create coupled spherical tensors of the form described above. These coupled basis elements are symmetrized with respect to the symmetry group of the spin system. For the analysis of the AX, AX_2, and AX_3 spin systems, only the symmetric spherical tensors are used to make up the basis set.

5. Once the fully coupled spherical tensor basis has been derived in terms of the single spin spherical tensor basis, a transformation matrix can be constructed between the Hamiltonian basis and the coupled spherical tensor basis.

6. In previous descriptions of the superspin formalism, this last matrix was used to convert between the two bases in order to determine the effects of pulses and delays. During a pulse, the density matrix was expressed in the spherical tensor basis and during a delay the density matrix was expressed in the Hamiltonian basis. The above transformation matrix illustrates the linear relationship between the two bases.

In the present analysis, the density matrix will be left in the spherical tensor basis, thus the last stage involves the derivation of general evolution formulae for the spherical tensors. This can be done using the results from the previous step, using the transformation between the spin space eigenvalues and the spherical tensors to express

each spherical tensor as a transformation between other spherical tensors with the same z component.

Thus using the spherical tensor basis a pulse is simply a rotation of the frame of reference, and a delay is a transformation amongst basis elements with a common coherence. The phase of a pulse describes the orientation of the magnetic field B_1 in the rotating frame, with respect to the x′ and y′ axes. The phase of the pulse is described by an angle ϕ, measured from the x axis, and is related to the γ and ϕ rotations about the Z and z′ axes during an Euler rotation. The effect of the phase of the pulse on a spin system is a multiplication of the density matrix elements by a factor:

$$e^{i\Delta m\phi}$$

where Δm is the change in coherence level brought about by the pulse. Thus the phase factor is related to the Wigner matrix elements by the difference in the subscripts, e.g. for the Wigner matrix element $d^1_{-11}(\theta)$ the phase factor would be $e^{2i\phi}$.

Appendix 2 shows the fully coupled basis for the AX, AX_2, and AX_3 systems in terms of the single spin spherical tensors. The form of these basis elements is that of two spherical tensors, the first one representing the A spins and the other representing the X spins:

$$|M_K)|M^S{}_s,k).$$

The fully coupled representation of the X spins is created by the symmetric combination of single spin spherical tensors the same way as one would combine angular momenta using Clebsch-Gordan coefficients. For example, in the two spin case:

$$|1_{+1},1) = \langle 11,00|11\rangle|1_{+1})|0) + \langle 00,11|11\rangle|0)|1_{+1}) \qquad [2.11]$$

The Clebsch-Gordan coefficients are described through the equation.[43]

$$\langle j_1 m_1 j_2 m_2 | JM \rangle = (-1)^{j_1 - j_2 + M}(2J+1)^{\frac{1}{2}} \begin{pmatrix} j_1 & j_2 & J \\ m_1 & m_2 & M \end{pmatrix} \qquad [2.12]$$

Here, j_1 and j_2 represent the angular momentum of the uncoupled spherical tensors and J is the total angular momentum of the coupled representation. Similarly, m_1, m_2 and M are the z components of the uncoupled and coupled representations. The term

$$\begin{pmatrix} j_1 & j_2 & J \\ m_1 & m_2 & M \end{pmatrix} \qquad [2.13]$$

is the Wigner 3j symbol, and these have been tabulated for many combinations of angular momentum.[46] The symmetrized spherical tensor $|1_{+1},1)$ is:

$$|1^S_{+1},1) = (2)^{-1/2}\{|1_{+1})|0) + |0)|1_{+1})\} \qquad [2.14]$$

The coupled spherical tensors are related to transition frequencies through another linear transformation. Through this transformation, formulae for the general evolution of the spherical tensors in Liouville spaced can be derived. These general evolution equations are equivalent to linear transformations which exchange coherence between spherical tensors with a common coherence level. It is these general evolution equations which make this study unique in the application of the superspin formalism, in that previous applications have performed the evolution of the magnetizations in the Hamiltonian basis, transforming back to the superspin basis to apply the pulses.[40]

A pulse sequence is made up of a series of pulses and delays which are applied

to a spin system. The effect of these pulses and delays can be determined mathematically using the formalism described above. The effect of a pulse is described by the Wigner matrix for that basis set, and is calculated by multiplying the appropriate Wigner matrix element by the corresponding density matrix element. When pulses are applied simultaneously to different nuclei in a spin system, the pulses are treated separately, with the net effect of the pulse being the multiplication of the density matrix by the product of the Wigner matrix elements for those pulses. During a delay, the density matrix is multiplied by the general evolution matrix. These steps are applied sequentially until the acquisition stage of the pulse sequence, where the evolution of the FID is described by the projection of the xy magnetization along the $|1_{+1})$ spherical tensor of the observed nucleus. In this study, the intensity of a line with respect to the delays was of interest, which is equivalent to the value of the $|1_{+1})$ tensor of the observed nucleus at the beginning of the acquisition period.

CHAPTER 3

BIRD Pulse Sequences

The short comings of the vector model show themselves in the description of BIRD pulse sequences (Figure 3.1). The BIRD sequence (or simply BIRD pulse) acts as a 180° pulse for protons bonded to ^{13}C and a 0° pulse for protons bonded to ^{12}C for one phase cycle, and the opposite case for another phase cycle.[35] This mechanism can be illustrated adequately using the vector picture for a single proton attached to either a ^{12}C or a ^{13}C, starting with the system at equilibrium (refer to figure 3.1). The x, x, x phase cycle will be illustrated. The initial 90°(H) pulse creates proton xy magnetization. The vectors associated with the $^1J_{CH}$ coupling in the $^1H^{13}C$ system will then begin to precess and dephase at $\nu_H \pm J_{CH}$. The delay τ is chosen so that these vectors will reach an antiphase orientation at the beginning of the 180°(C,H) pulses. The 180° proton pulse is applied along the x axis and will have no effect on these vectors because they are also aligned along the x axis. The carbon 180° pulse will cause the vectors to refocus at the end of the next delay τ. At the beginning of the final proton 90° pulse the vectors will be refocussed along the y axis, and the application of the pulse along the x axis will bring these vectors down along the -z axis, thus the net effect of the sequence is a proton 180° pulse. The protons bonded to the ^{12}C will not dephase during the first delay τ, so the

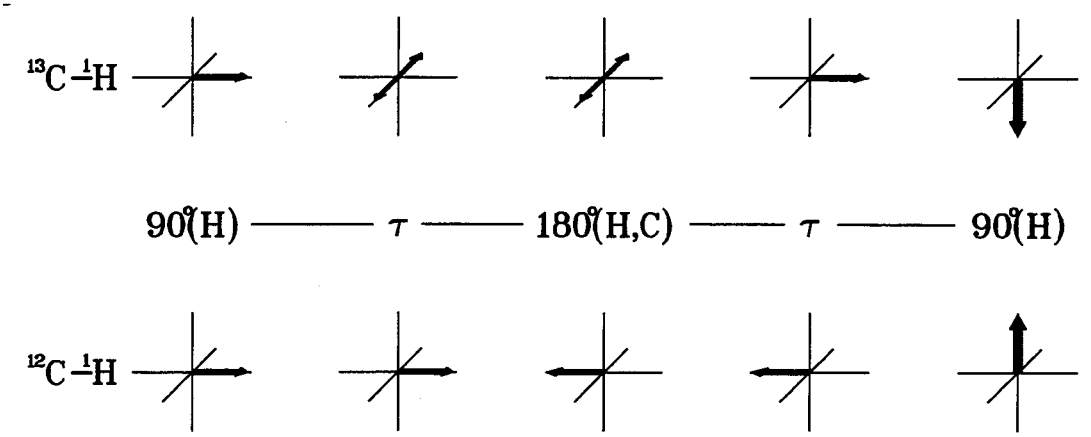

Figure 3.1. Vector diagram showing evolution of coherence in ^{13}C-^{1}H system (top) and ^{12}C-^{1}H system (bottom) during a BIRD sequence.

proton 180° pulse will transfer the magnetization to the -y axis. The final proton 90° pulse along the x axis will bring the magnetization back up along the z axis, having the net effect of a 0° pulse.

This picture of a BIRD pulse falls short however, when describing more complex spin systems, particularly when the system is not at equilibrium at the beginning of the pulse. The vector model fails to illustrate the evolution of multiple quantum levels during the delays of the BIRD pulse, and gives little insight to the effect that the choice of this delay has on the net effect of the BIRD pulse. Most applications involving BIRD pulses use the sequence when the system is not at equilibrium, either after the initial proton magnetization has been created, or after polarization transfer. In complex systems the initial 90° pulse will create multiple quantum coherence depending on the number of nuclei in the spin system (e.g. an AX_3 system can have quad quantum levels.). These multiple quantum levels will then evolve at their characteristic frequency during the delays in the BIRD sequence. Certain of these transitions will be refocussed after the

180° pulses but there will be some magnetization transferred back to an observable level by the final 90° pulse that evolved during a multiple quantum level and has passed on some of this dependence to the observable level. This can have dramatic effects on the intensity of the magnetization that is detected after the BIRD sequence, with respect to the interpulse delay, τ.

In order to study the effects of the parameters of the BIRD sequence on a system that is not at equilibrium, a pulse sequence was created from the refocussed INEPT experiment. The BIRD pulse was used in place of the refocussing 180° pulse to study the BIRD pulse on systems after polarization had been transferred to the carbons. This situation occurs in pulse sequences such as the FLOCK sequence[47] where the BIRD pulse is used freely to help increase the sensitivity of long range correlation experiments.

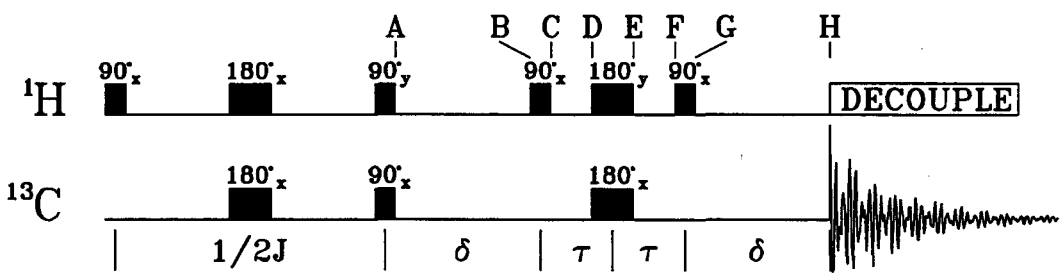

Figure 3.2. INEPT-BIRD pulse sequence. BIRD pulse has replaced refocussing 180° pulse from the INEPT experiment. Labels show the landmark points referred by the text.

In the INEPT-BIRD pulse sequence there will be all carbon coherence at the beginning of the BIRD pulse, resulting from the polarization transfer from INEPT. The analysis will start at the point immediately following polarization transfer, and follow the coherence through the BIRD pulse up to the point of acquisition. In figure 3.2, letters label the points where pulses and delays begin and end, and the values of the density

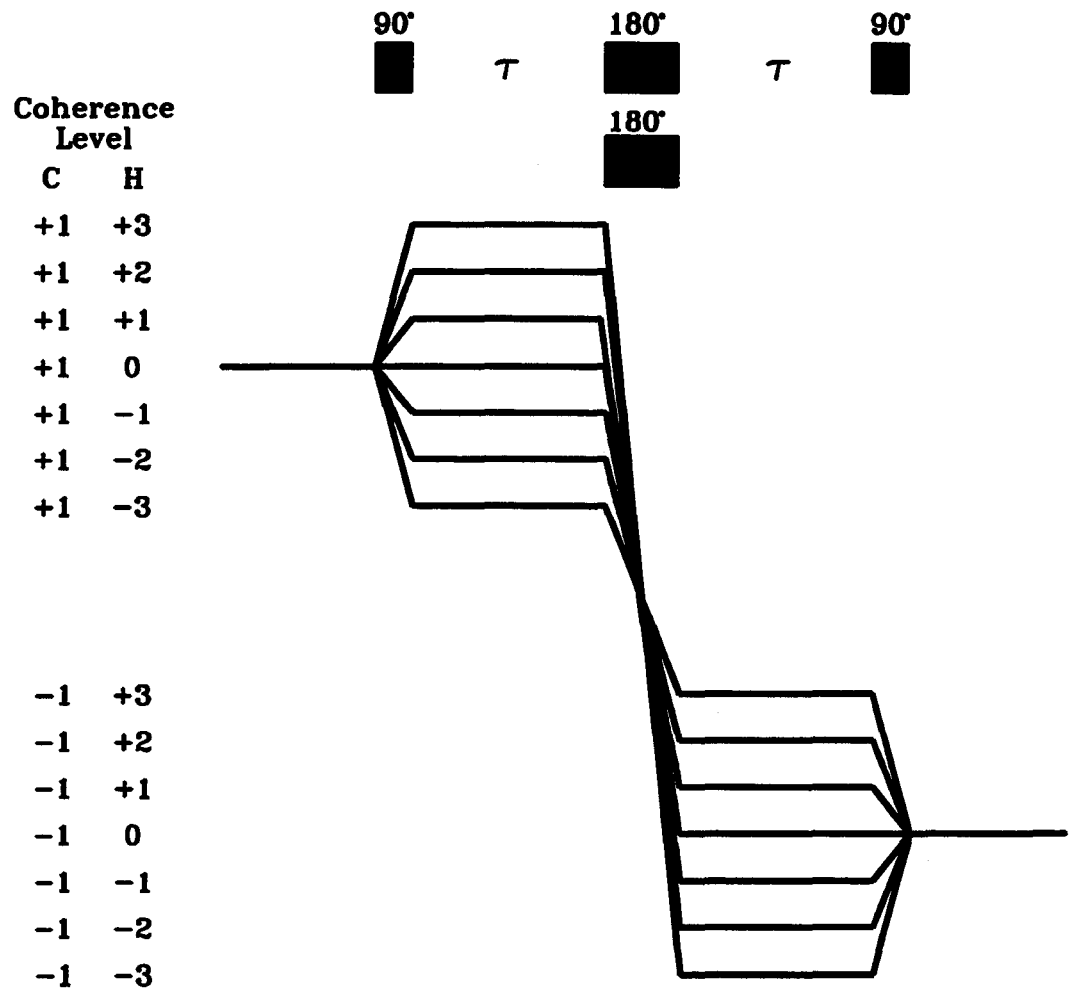

Figure 3.3. Coherence transfer pathway for the AX_3 system.

matrix elements at these points are denoted by this letter in superscript after the notation for that spherical tensor. Even though the protons are in a zero quantum level, the subsequent delay after polarization transfer will create levels with angular momentum greater than zero. The application of a 90° pulse to this will result in the creation of multiple quantum coherence. The creation of the multiple quantum levels and their evolution can be followed through the aid of the coherence transfer pathway in figure 3.3.[48,49] The following analysis will make reference to the pulse sequence in figure 3.2,

using the letter labels as landmarks for the analysis.

In terms of the superspin formalism, the following density matrix elements will have non-zero intensity at the beginning of the BIRD sequence in an AX_2 system:

$$|\mathbf{1}_{+1})|\mathbf{0,0})^{B} \quad [3.1]$$

$$|\mathbf{1}_{+1})|\mathbf{0,2})^{B} \quad [3.2]$$

$$|\mathbf{1}_{+1})|\mathbf{1}_{0},\mathbf{1})^{B} \quad [3.3]$$

$$|\mathbf{1}_{+1})|\mathbf{2}_{0},\mathbf{2})^{B} \quad [3.4]$$

The initial 90°(H) pulse in the BIRD sequence will act as a rotation of the frame of reference in the superspin formalism. This rotation is described by the Wigner rotation matrices $d^{n}(\theta)$, where n represents the angular momentum of the transition (or superspin), and θ is the angle of the rotation (or pulse angle). Thus for the AX_2 system the rotation matrix is made up of the Wigner matrices d^0, d^1, and d^2.[43,50-52] The action of a pulse on a system is described by multiplying the density matrix of superspin elements by the corresponding rotation matrix:

$$\rho^{+} = \boldsymbol{D}\bullet\rho^{-} \quad [3.5]$$

where ρ^{-} and ρ^{+} are the density matrices before and after the pulse,

$\boldsymbol{D}$ is the total rotation matrix = $d^0 \oplus d^1 \oplus d^2$

These individual rotation matrices are made up of elements denoted by:

$$d^{J}_{M',M}(\theta) \quad [3.6]$$

where J is the total angular momentum of the transition, M′ is the z-component of the final state and M is the z-component of the initial state.[43] θ is the Euler angle representing the rotation from the Z axis. When a rotation acts on an eigenstate $|\mathbf{J}_{M})$,

it cannot change the value of the total angular momentum J, but can only transform $|J_M)$ into a linear combination of other M values. The consequences of this in superspin are that a pulse can only change the coherence level of a transition, leaving the superspin, or the total angular momentum of the transition, alone. The amount of coherence that gets transferred into other coherence levels is governed by the Wigner matrix elements. The Wigner matrices are arranged so that elements increase in M′ from left to right along the rows of the matrix, and increase in M down the columns of the matrix. For a 90° pulse acting on the AX_2 system, the rotation matrices will have the following values:

$$d^0\left(\frac{\pi}{2}\right) = (1) \qquad [3.7]$$

$$d^1\left(\frac{\pi}{2}\right) = \begin{pmatrix} \frac{1}{2} & -\frac{1}{\sqrt{2}} & \frac{1}{2} \\ \frac{1}{\sqrt{2}} & 0 & -\frac{1}{\sqrt{2}} \\ \frac{1}{2} & \frac{1}{\sqrt{2}} & \frac{1}{2} \end{pmatrix} \qquad [3.8]$$

$$d^2\left(\frac{\pi}{2}\right) = \begin{pmatrix} \frac{1}{4} & \frac{1}{2} & \sqrt{\frac{3}{8}} & -\frac{1}{2} & \frac{1}{4} \\ \frac{1}{2} & -\frac{1}{2} & 0 & \frac{1}{2} & -\frac{1}{2} \\ \sqrt{\frac{3}{8}} & 0 & -\frac{1}{2} & 0 & \sqrt{\frac{3}{8}} \\ \frac{1}{2} & \frac{1}{2} & 0 & -\frac{1}{2} & -\frac{1}{2} \\ \frac{1}{4} & -\frac{1}{2} & \sqrt{\frac{3}{8}} & \frac{1}{2} & \frac{1}{4} \end{pmatrix} \qquad [3.9]$$

Since all of the proton magnetizations are in zero quantum levels the only rotation matrix elements that are used are those with M = 0. The amount of coherence that gets transferred to any level is determined by the Wigner matrix elements. Thus the changes

in coherence will be as follows:

$$|1_{+1}\rangle|0,0\rangle^C = d^0_{00}|1_{+1}\rangle|0,0\rangle^B \qquad \text{(single quantum coherence)}$$

$$|1_{+1}\rangle|0,2\rangle^C = d^0_{00}|1_{+1}\rangle|0,2\rangle^B \qquad \text{(single quantum coherence)}$$

$$|1_{+1}\rangle|1_{+1},1\rangle^C = d^1_{10}|1_{+1}\rangle|1_0,1\rangle^B \qquad \text{(double quantum coherence)}$$

$$|1_{+1}\rangle|1_{-1},1\rangle^C = d^1_{-10}|1_{+1}\rangle|1_0,1\rangle^B \qquad \text{(zero quantum coherence)}$$

$$|1_{+1}\rangle|2_0,2\rangle^C = d^2_{00}|1_{+1}\rangle|2_0,2\rangle^B \qquad \text{(single quantum coherence)}$$

$$|1_{+1}\rangle|2_{+2},2\rangle^C = d^2_{20}|1_{+1}\rangle|2_0,2\rangle^B \qquad \text{(triple quantum coherence)}$$

$$|1_{+1}\rangle|2_{-2},2\rangle^C = d^2_{-20}|1_{+1}\rangle|2_0,2\rangle^B \qquad \text{(single quantum coherence)}$$

Note that there is no coherence transferred to the $|1_{+1}\rangle|1_0,1\rangle$, $|1_{+1}\rangle|2_{+1},2\rangle$ and $|1_{+1}\rangle|2_{-1},2\rangle$ levels because the Wigner matrix elements $d^1_{00}(\pi/2)$, $d^2_{10}(\pi/2)$ and $d^2_{-10}(\pi/2)$ are all zero. Thus the 90°(^{1}H) pulse has created zero, single, double and triple quantum coherence.

These multiple quantum levels will evolve over the first interpulse delay, τ, in the BIRD pulse, according to the general evolution formulae derived earlier. During the delay, the coherence level, or the z component of the angular momentum, remains constant, however the total angular momentum may change. Thus transitions that share a common coherence level may transfer angular momentum during the course of the delay, and transitions that had zero intensity at the beginning of the delay may have considerable intensity at the end of the delay. In this manner, the duration of the delay allows one to choose which transitions will survive to the end of the pulse sequence and be detected.

The evolution of the transitions is shown in terms of the intensity of the transitions

at the end of the first interpulse delay. In practice, a discrete value of τ would be chosen in order to optimise the intensity, or some other property of the spectrum, however in this study the dependence of the detected signal on the interpulse delay is of interest, so the value of the time interval is kept general. The density matrix elements evolve according to the formulae outlined in the appendix, and in the results below the effects of the delay δ have been evaluated, where the effects of the interpulse delay have intentionally been left in the form from the general evolution formulae to illustrate the source of the evolution. The intensity of the transitions in terms of τ are:

$$|1_{+1}|0,0)^D = ie^{i\nu_A\delta}e^{i\nu_A t}\sin J\delta[\frac{1}{2\sqrt{2}}(1+\cos J\tau) - \frac{1}{6\sqrt{2}}(1-\cos J\tau) + \frac{1}{6\sqrt{2}}(1-\cos J\tau)] \quad [3.10]$$

$$|1_{+1}|1_0,1)^D = -e^{i\nu_A\delta}e^{i\nu_A\tau}\sin J\delta[-\frac{1}{2}(1-\cos J\tau) - \frac{1}{6}\sin J\tau + \frac{1}{6}\sin J\tau] \quad [3.11]$$

$$|1_{+1}|0,2)^D = ie^{i\nu_A\delta}e^{i\nu_A t}\sin J\delta[\frac{1}{2\sqrt{6}}(1-\cos J\tau) - \frac{1}{6\sqrt{6}}(5+\cos J\tau) - \frac{1}{6\sqrt{6}}(1-\cos J\tau)] \quad [3.12]$$

$$|1_{+1}|2_0,2)^D = ie^{i\nu_A\delta}e^{i\nu_A t}\sin J\delta[-\frac{1}{2\sqrt{3}}(1-\cos J\tau) - \frac{1}{6\sqrt{3}}(1-\cos J\tau) - \frac{1}{6\sqrt{3}}(2+\cos J\tau)] \quad [3.12]$$

$$|1_{+1}|1_{-1},1)^D = \frac{1}{\sqrt{2}}e^{i\nu_A\delta}e^{i(\nu_A-\nu_X)\tau}\cos J\delta\cos\frac{1}{2}J\tau \quad [3.13]$$

$$|1_{+1}|2_{-1},2)^D = \frac{i}{\sqrt{2}}e^{i\nu_A\delta}e^{i(\nu_A-\nu_X)\tau}\cos J\delta\sin\frac{1}{2}J\tau \quad [3.14]$$

$$|1_{+1}|1_{+1},1)^D = -\frac{1}{\sqrt{2}}e^{i\nu_A\delta}e^{i(\nu_A+\nu_X)\tau}\cos J\delta\cos\frac{1}{J}\tau \quad [3.15]$$

$$|1_{+1}|2_{+1},2)^D = \frac{i}{\sqrt{2}}e^{i\nu_A\tau}e^{i(\nu_A+\nu_X)\delta}\cos J\delta\sin\frac{1}{2}J\tau \quad [3.16]$$

$$|1_{+1}\rangle|2_{+2},2\rangle^{D} = \frac{i}{2\sqrt{2}}e^{i\nu_A\delta}e^{i(\nu_A+2\nu_X)\tau}\sin J\delta \qquad [3.17]$$

$$|1_{+1}\rangle|2_{-2},2\rangle^{D} = \frac{i}{2\sqrt{2}}e^{i\nu_A\delta}e^{i(\nu_A-2\nu_X)\tau}\sin J\delta \qquad [3.18]$$

In the superspin formalism, the simultaneous 180°(H,C) pulses will reverse the sign of the coherence level of all of the transitions, in both the carbon and proton domains. For a 180° pulse, the Wigner rotation matrices simplify to:

$$d^{0}(\pi) = (1) \qquad [3.19]$$

$$d^{1}(\pi) = \begin{pmatrix} 0 & 0 & 1 \\ 0 & -1 & 0 \\ 1 & 0 & 0 \end{pmatrix} \qquad [3.20]$$

$$d^{2}(\pi) = \begin{pmatrix} 0 & 0 & 0 & 0 & 1 \\ 0 & 0 & 0 & -1 & 0 \\ 0 & 0 & 1 & 0 & 0 \\ 0 & -1 & 0 & 0 & 0 \\ 1 & 0 & 0 & 0 & 0 \end{pmatrix} \qquad [3.21]$$

The pulses can be applied to the carbon and proton channels independently, with the net amount of coherence transfer for each transition represented by the product of the corresponding Wigner matrix elements. For example, the net effect of the 180°(H,C) pulse on the $|1_{+1}\rangle|2_{+1},1\rangle$ transition would be:

$$|1_{-1}\rangle|2_{-1},1\rangle = d^{1}_{-11}(\pi)d^{2}_{-11}(\pi)|1_{+1}\rangle|2_{+1},1\rangle \qquad [3.22]$$

The effect in terms of the physics of the density matrix is that all transitions from

before the 180°(H,C) pulse will be transferred to their counterparts which are rotating at the opposite frequency. Thus at the end of the last τ delay, any frequency dependent term in the description of the density matrix will cancel out by the end of the pulse sequence. However in the expressions for the general evolution of the transitions, there are terms which will have different evolutions before and after the 180°(H,C) pulses. For example, before the pulses, the evolution of $|\mathbf{1}_{+1}|\mathbf{0,0})$ over τ was:

$$|1_{+1})|0,0) = e^{i\nu_A\tau}[\tfrac{1}{2}(1+\cos J\tau)|1_{+1})|0,0) - \tfrac{1}{\sqrt{6}}(1-\cos J\tau)|1_{+1})|2_0,2) + \tfrac{1}{2\sqrt{3}}(1-\cos J\tau)|1_{+1})|0,2)] \quad \textbf{[3.23]}$$

However, during the first interpulse delay, the transition $|\mathbf{1}_{+1}|\mathbf{1}_0,\mathbf{1})$ was created, but did not contribute to the evolution of the $|\mathbf{1}_{+1}|\mathbf{0,0})$ transition because it had zero intensity at the beginning of the delay. This transition will be transferred to $|\mathbf{1}_{-1}|\mathbf{1}_0,\mathbf{1})$ by the 180°(H,C) pulse, and this will then contribute to the evolution of the $|\mathbf{1}_{-1}|\mathbf{0,0})$ level and to the other transitions with zero coherence in the proton domain. Thus after the 180°(H,C) pulses the evolution of $|\mathbf{1}_{-1}|\mathbf{0,0})$ will be made up of 4 transitions from before the pulse:

$$|1_{-1})|0,0) = e^{-i\nu_A\tau}[\tfrac{1}{2}(1+\cos J\tau)|1_{+1})|0,0) - \tfrac{i}{\sqrt{2}}\sin J\tau)|1_{+1})|1_0,1) - \tfrac{1}{\sqrt{6}}(1-\cos J\tau)|1_{+1})|2_0,2) + \tfrac{1}{2\sqrt{3}}(1-\cos J\tau)|1_{+1})|0,2)] \quad \textbf{[3.24]}$$

In order to simplify the analysis, the number of transitions that need to be followed from this point can be reduced by analyzing only the transitions that will contribute to the observable level. At the receiver, the only level that can be detected is the $|\mathbf{1}_{-1}|\mathbf{0,0})$ level, since this experiment is designed to acquire in the carbon channel

and the $|1_{+1}\rangle$ and $|1_{-1}\rangle$ transitions represent transverse magnetization in the x'y' plane. Thus during the last refocussing delay during the INEPT-BIRD experiment, the only transition that needs to be followed is the $|1_{-1}|0,0\rangle$ level. Additionally, this means that transitions evolving during the last interpulse delay and through the last 90° pulse that will contribute to the evolution of the $|1_{+1}|0,0\rangle$ level during the refocussing delay need to be followed after the 180°(H,C) pulse. It can be seen from the equation above, that the only levels that will contribute to the observable level are the $|1_{-1}|0,0\rangle$, $|1_{-1}|1_0,1\rangle$, $|1_{-1}|0,2\rangle$ and $|1_{-1}|2_0,2\rangle$ levels. These levels are created by the final 90°(H) pulse, which transfers coherence from several levels, including multiple quantum levels, to make up the intensity of the received transition. The intensity of the single quantum transition after the 90°(H) pulse can be expressed in terms of the transitions before the pulse and their corresponding Wigner matrix elements:

$$|1_{-1}|0,0\rangle^G = d^0_{00}(\pi/2)|1_{-1}|0,0\rangle^F \qquad [3.25]$$

$$|1_{-1}|0,2\rangle^G = d^0_{00}(\pi/2)|1_{-1}|0,2\rangle^F \qquad [3.26]$$

$$|1_{-1}|1_0,1\rangle^G = d^1_{01}(\pi/2)|1_{-1}|1_{+1},1\rangle^F + d^1_{0\text{-}1}(\pi/2)|1_{-1}|1_{-1},1\rangle^F \qquad [3.27]$$

$$|1_{-1}|2_0,2\rangle^G = d^2_{00}(\pi/2)|1_{-1}|2_0,2\rangle^F + d^2_{02}(\pi/2)|1_{-1}|2_{+2},2\rangle^F + d^2_{0\text{-}2}(\pi/2)|1_{-1}|2_{-2},2\rangle^F \qquad [3.28]$$

As can be seen from the above equations, the $|1_{-1}|1_0,1\rangle$, $|1_{-1}|2_{-1},2\rangle$ and $|1_{-1}|2_{+1},2\rangle$ levels do not contribute directly to the intensity of the observed signal, however the intensity of these transitions at the beginning of the final interpulse delay contribute to the evolution of other levels that appear in the final coherence.

The evolution during τ in the second half of the BIRD sequence succeeds in

removing any chemical shift dependence from the evolution of the transitions. This arises because of the effect of the 180°(H,C) pulse in transferring the coherences to their counterrotating elements. The chemical shift dependence is described by an exponential term in the general evolution equation for that coherence, and counterrotating terms will differ by the sign of the exponent. The exponential terms from before the pulse will cancel out with the exponential terms after the pulse. This simplifies the time dependence of the transitions to a case which has no chemical shift dependence, or is essentially at resonance.

The evolution of the transitions after the 180°(H,C) pulse follow the equations in appendix 3. Only the transitions that contribute to the detected signal will be shown here. At the beginning of the final 90°(H) pulse the intensity of the signals of interest will be:

$$|1_{-1}\rangle|0,0\rangle^F = \frac{1}{2\sqrt{2}}1e^{i\nu_A\delta}\sin J\delta(1+\cos 2J\tau) \qquad [3.29]$$

$$|1_{-1}\rangle|0,2\rangle^F = -\frac{1}{2\sqrt{6}}ie^{i\nu_A\delta}\sin J\delta(1+\cos 2J\tau) \qquad [3.30]$$

$$|1_{-1}\rangle|2_0,2\rangle^F = -\frac{1}{2\sqrt{3}}ie^{i\nu_A\delta}\sin J\delta \qquad [3.31]$$

$$|1_{-1}\rangle|1_{+1},1\rangle^F = -\frac{1}{\sqrt{2}}e^{i\nu_A\delta}\cos J\delta\cos J\tau \qquad [3.32]$$

$$|1_{-1}\rangle|1_{-1},1\rangle^F = \frac{1}{\sqrt{2}}e^{i\nu_A\delta}\cos J\delta\cos J\tau \qquad [3.33]$$

$$|1_{-1}\rangle|2_{+2},2\rangle^F = \frac{1}{2\sqrt{2}}ie^{i\nu_A\delta}\sin J\delta \qquad [3.34]$$

$$|1_{-1}\rangle|2_{-2},2\rangle^F = \frac{1}{2\sqrt{2}}ie^{i\nu_A\delta}\sin J\delta \qquad [3.35]$$

All of the above levels will be transferred to zero quantum proton coherence levels by the final 90°(H) pulse. The evolution of the observed level will depend upon the value of all of the zero quantum proton coherences after this pulse:

$$|1_{-1}\rangle|0,0\rangle^G = |1_{-1}\rangle|0,0\rangle^F = \frac{1}{2\sqrt{2}} ie^{i\nu_A\delta} \sin J\delta(1+\cos 2J\tau) \qquad [3.36]$$

$$|1_{-1}\rangle|0,2\rangle^G = |1_{-1}\rangle|0,2\rangle^F = \frac{1}{2\sqrt{6}} ie^{i\nu_A\delta} \sin J\delta(1+\cos 2J\tau) \qquad [3.37]$$

$$|1_{-1}\rangle|1_0,1\rangle^G = \frac{1}{\sqrt{2}}|1_{-1}\rangle|1_{+1},1\rangle^F - \frac{1}{\sqrt{2}}|1_{-1}\rangle|1_{-1},1\rangle^F = e^{i\nu_A\delta}\cos J\delta\cos J\tau \qquad [3.38]$$

$$|1_{-1}\rangle|2_0,2\rangle^G = -\frac{1}{2}|1_{-1}\rangle|2_0,2\rangle^F + \sqrt{\frac{3}{8}}|1_{-1}\rangle|2_{+2},2\rangle^F + \sqrt{\frac{3}{8}}|1_{-1}\rangle|2_{-2},2\rangle^F = \frac{1}{\sqrt{3}} ie^{i\nu_A\delta}\sin J \qquad [3.39]$$

The observed level will then evolve according to the formula in appendix 1, giving the functional form for the intensity of the carbon signal in an AX_2 system as a function of δ and τ. This final evolution will then remove the chemical shift dependence of δ, and the final functional form will have no chemical shift dependence:

$$\begin{aligned} |1_{-1}\rangle|0,0\rangle^H = i\sin J\delta[&\frac{1}{6\sqrt{2}}(1+2\cos J\delta)(1+\cos 2J\tau) \\ &+ \frac{1}{\sqrt{2}}\cos J\delta\cos J\tau \\ &- \frac{1}{3\sqrt{2}}(1-\cos J\delta)] \end{aligned} \qquad [3.40]$$

Figures 3.4, 3.5 and 3.6 illustrate the dependence of the carbon intensity on the BIRD interpulse delay. This data is derived from simulations[53] of the INEPT-BIRD sequence performed on AX, AX_2, and AX_3 systems, with J_{AX} equal to 125 Hz. From

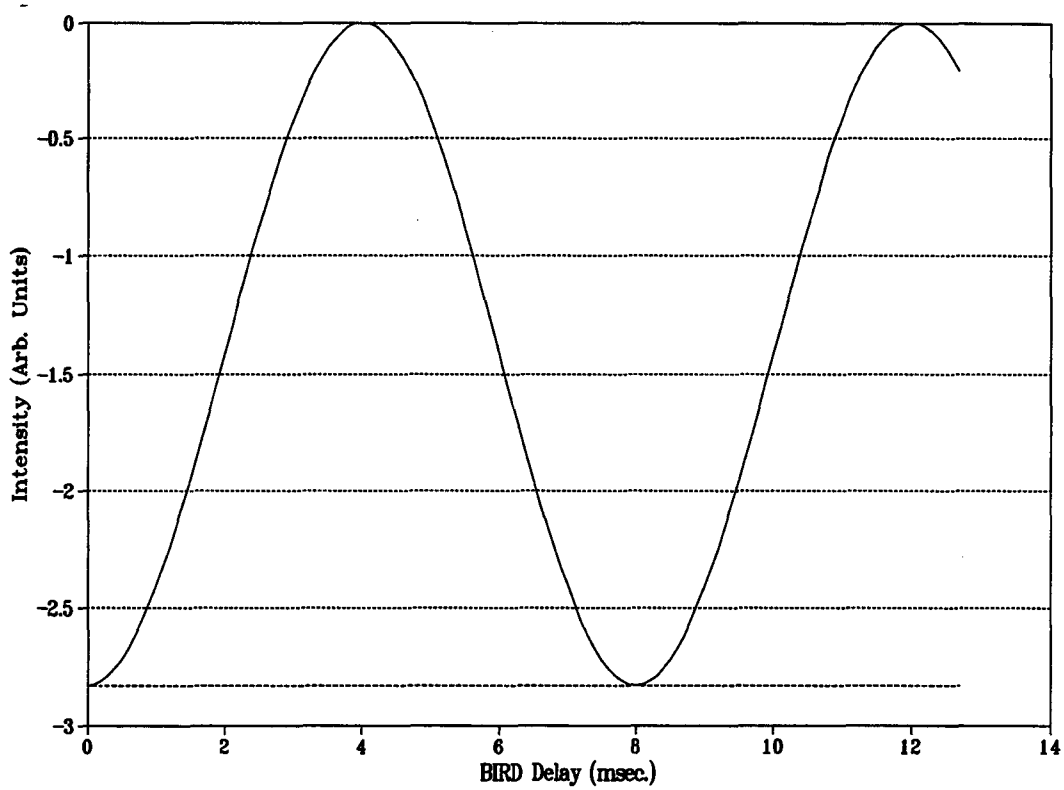

Figure 3.4 Intensity variation of carbon signal in AX system with respect to BIRD delay in INEPT-BIRD experiment (solid line) and refocussed INEPT intensity (broken line).

these simulations it can be seen that the intensity of the carbon signal is maximized when the BIRD pulse acts as a 180° pulse, i.e. when the interpulse delay is zero, and when the BIRD delay is optimized for J_{AX}. In all these cases the intensity through the INEPT-BIRD experiment is identical to that obtained from the refocussed INEPT experiment. When the BIRD delay is not optimized, in all cases there is a null at $\tau = 1/2J_{AX}$. In the AX system the dependence is a simple sinusoid, varying between maxima at $(2n)/2J_{AX}$ and minima at $(2n+1)/2J_{AX}$. In the AX_2 and AX_3 systems the dependence becomes more complex, with increasingly narrower maxima as the number of X nuclei increase. At $\tau = 1/2J_{AX}$, the intensity variation becomes even more complex with higher spin systems

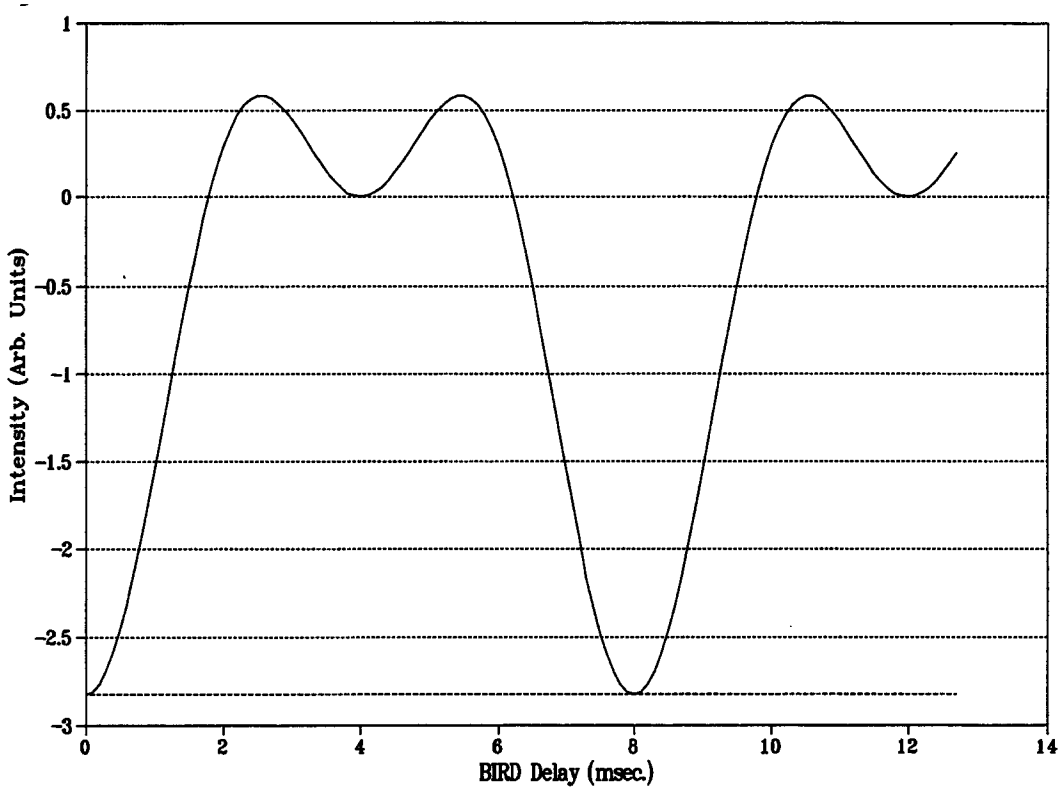

Figure 3.5 Intensity variation of carbon signal in AX_2 system with respect to BIRD delay in INEPT-BIRD experiment (solid line) and refocussed INEPT intensity (broken line)

showing a broader range of near zero values. The AX_3 system shows three null points in each cycle with the narrowest region of maximum intensity. This would indicate that the AX_3 system is most sensitive to the selection of the BIRD delay. The complex intensity variation around the null region implies that with the correct selection of BIRD delay that this could be taken advantage of for spectral editing, however the signal intensities around this point would be very low, possibly indistinguishable from noise.

There is also a phase cycle dependence upon this effect, which in the AX picture, differentiates between the BIRD pulse acting as a 180° pulse for a proton coupled to a ^{13}C for the x, x, x phase cycle, and acting as a 0° pulse for this same proton in the x, x, -

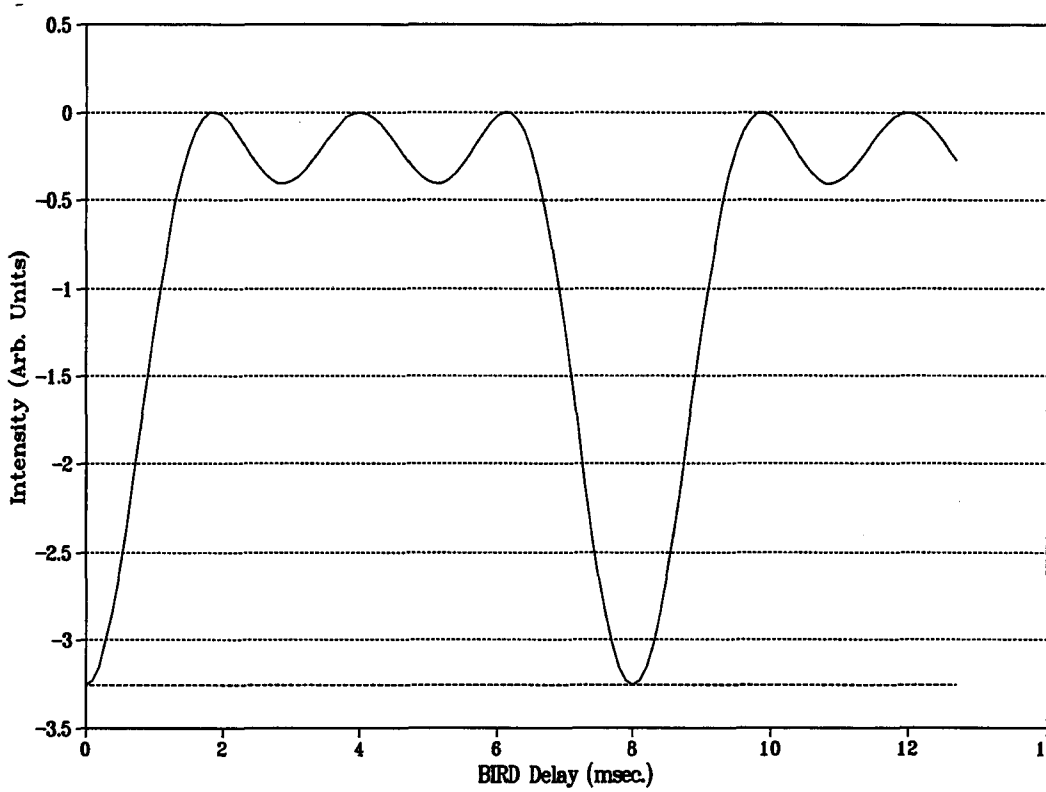

Figure 3.6 Intensity variation in carbon signal in AX_3 system with respect to BIRD delay in INEPT-BIRD experiment (solid line) and refocussed INEPT intensity (broken line).

x phase cycle. In the analysis of the BIRD sequence on the AX, AX_2 and AX_3 systems, this phase cycle difference manifests itself as a phase shift in the variation of the carbon signal intensity. In the x, x, x phase cycle, the signal intensity is a maximum at an interpulse delay of 0 and null at an interpulse delay of $1/2J_{AX}$. With the opposite phase cycle, the null and maxima occur at opposite points. Figure 3.7 shows the difference between the two phase cycles for the AX_2 system.

In addition, in the AX_2 and AX_3 systems, the region about the null broadens, and the maxima narrows. This makes the choice of interpulse delay (τ) more critical in higher spin systems, as there is a narrower range of values of τ which show a measurable

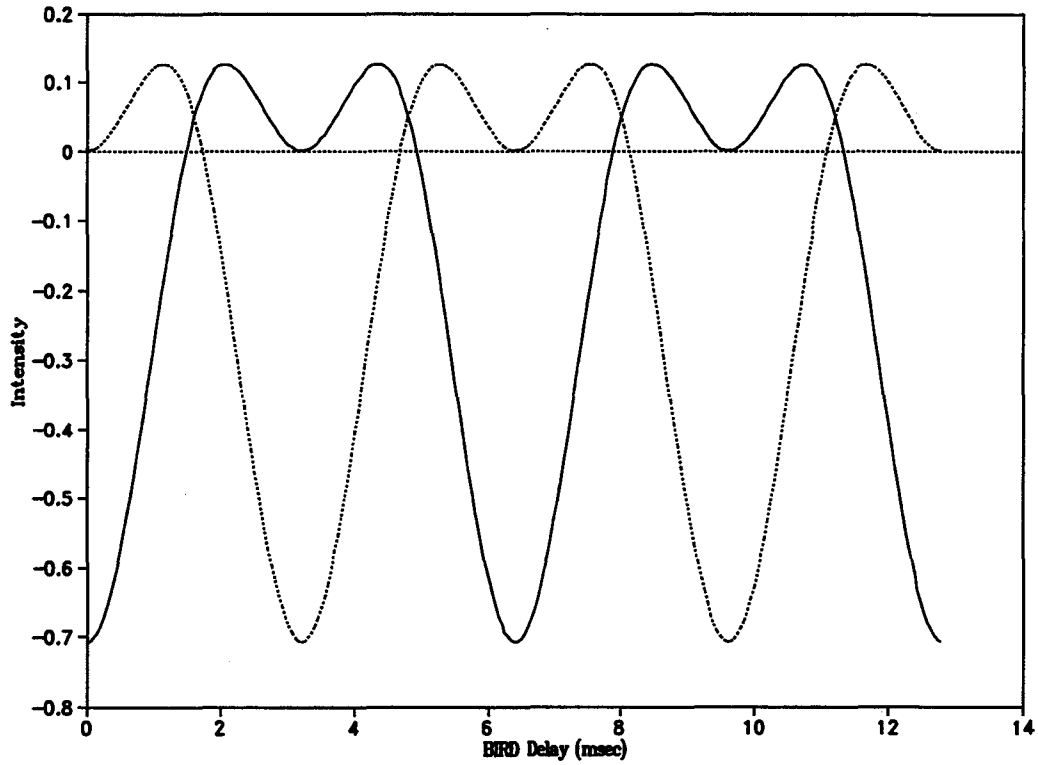

Figure 3.7: Comparison of intensity variation of carbon signal in AX_2 system with phase cycle of BIRD sequence. Solid line: x, x, -x; dotted line x, x, x.

signal. The broad null regions could be used to separate signals of higher order spin systems (AX_3) from lower order spin systems (AX) by nulling the AX_3 signal at a point where an AX signal has higher intensity. This idea could be taken further by combining pulse sequences with different phase cycles used to create AX signals with opposite intensity of AX_2 signals. Thus spin sorting could be done in two dimensional spectra using the interpulse delay and phase of BIRD pulses. Figure 3.8 shows the result of adding together signals from both the x, x, x phase cycle and the x, x, -x phase cycle for the AX and AX_2 spin systems. The AX signal shows no modulation with changes in the BIRD interpulse delay, the signal is always positive. The AX_2 signal has a sinusoidal

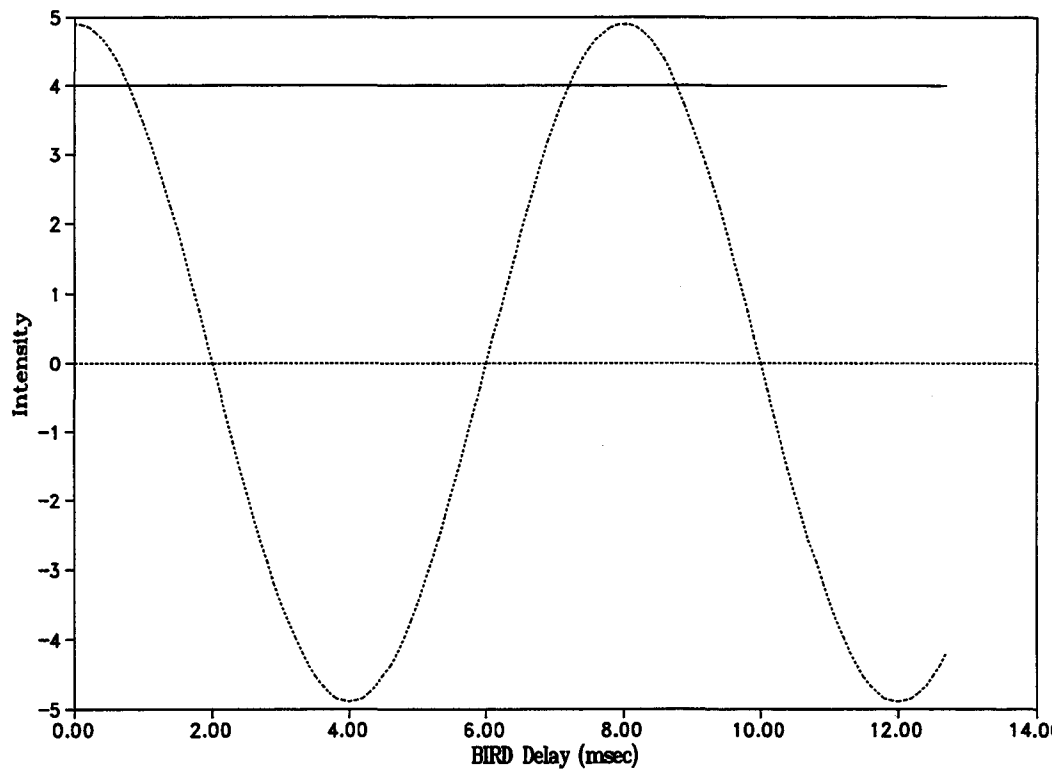

Figure 3.8: Comparison of AX signal intensity (solid line), and AX_2 signal intensity (dotted line) by taking the difference between the x, x, x and x, x, -x phase cycles.

modulation with respect to the interpulse delay, which means that a delay could be chosen that would give a two dimensional spectrum with positive AX lines and negative AX_2 lines.

Chapter 4

Artifacts in 2-dimensional Heteronuclear Shift Correlated Spectra

Artifacts in NMR spectra have been described almost since the beginning of pulsed NMR. Many of these artifacts have been associated with experimental conditions such as sweep width or pulse width error.[54-56] In the early days of two dimensional NMR many of these artifacts could be eliminated through creative phase cycling procedures, or through the use of composite pulses.[49,57,58] Other artifacts however can be attributed to systematic factors, which cannot be eliminated in this manner. Some are a result of the nature of the spin system, such as virtual coupling,[59-62] and can lead to false correlations in two dimensional spectra, and others are a result of the effect of the pulse sequence on certain spin systems, such as in methylene systems in decoupled heteronuclear shift correlation spectra.[63] These artifacts are persistent and can be predicted through a rigorous mathematical treatment of the pulse experiment on the spin system.

This section of this work outlines the use of the superspin formalism to determine a functional form describing the appearance of an artifact associated with strongly coupled methylene systems during heteronuclear shift correlation experiments which use a constant time period during the t_1 evolution in order to effect homonuclear decoupling in the

proton domain. Two pulse sequences will be studied here, one in detail, the COLOC experiment,[36] which will be analyzed using the superspin formalism,[37] and one which employs a BIRD sequence to help refocus long range couplings and improve sensitivity. The second experiment, known as HETRES,[64,65] will be analyzed using computer simulations which make use of the superspin formalism.[53]

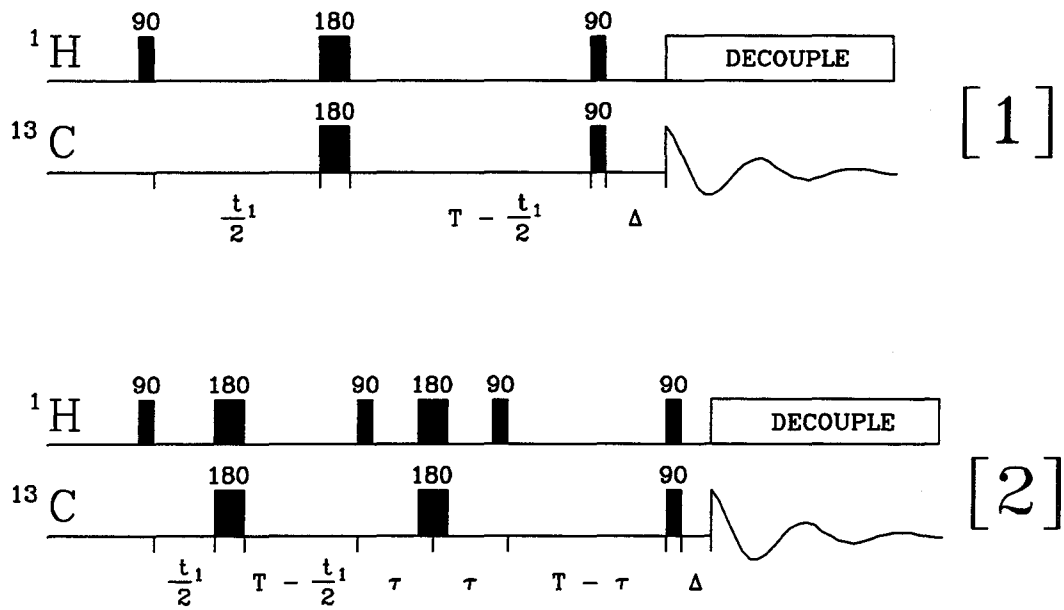

Figure 4.1: Pulse sequences used in this study: [1] COLOC and [2] HETRES pulse sequences.

Heteronuclear chemical shift correlation experiments were reviewed in the introduction to this thesis. The common attribute amongst the pulse sequences studied in this section are that they achieve broadband decoupling in f_1 through the use of a constant time between initial excitation and acquisition. The COLOC experiment[36] is a popular variant of this, used in both long range and direct bonded heteronuclear correlation spectroscopy. In the direct bonded COLOC experiment,[66] the resolution is limited by the length of the constant time period, T, which is restricted by the value of

the $^{1}J_{CH}$. To increase resolution, this can be increased by odd multiples of $1/(2^{1}J_{CH})$. However, as the time period increases, the sensitivity can be adversely effected by the $^{n>1}J_{CH}$ reaching an antiphase orientation at the time of polarization transfer.[66,67] A modification of the COLOC experiment is to place a BIRD pulse sequence[35] at time T, and extend the pulse sequence for a further time T-τ, where τ is the interpulse delay in the BIRD sequence.[64,65] The BIRD pulse acts as a ^{1}H 180° pulse for protons bonded to ^{13}C, therefore vicinal proton-proton couplings will be refocussed at the time of polarization transfer, effectively decoupling the vicinal protons from the directly bonded protons in f_1.

In this study, the effect of the HETRES and COLOC pulse sequences will be studied as applied to methylene systems with inequivalent protons. The HETRES experiment should effect proton-proton decoupling between the methylene protons in f_1 providing the constant time period, 2T-τ, is chosen as an odd multiple of $1/(2^{1}J_{CH})$. The methylene correlation spectrum should consist of two peaks representing the chemical shift of each of the methylene protons. The spectrum actually consists of three peaks, the third occurring at the average frequency of the methylene chemical shift, and with an intensity modulated by the chemical shift difference between the two protons. Artifacts associated with inequivalent methylene systems have been observed before associated with other experiments, and in many cases are associated with experiments which attempt proton-proton decoupling.[65,68-73]

The intensity of the artifact peak was analyzed in the COLOC experiment through the use of the superspin formalism.[37,40-42] The methylene system is approximated using

an ABX spin system. The methods used in the calculations are similar to those outlined in the previous chapter,[40,74] with the exception that the evolutions for the ABX system are done by transforming the density matrix to the Hamiltonian basis and applying the evolution, then transforming back to the superspin basis for the pulses. It is assumed that the effects of the BIRD sequence is negligible, since the BIRD delays are very small compared to the evolution of the homonuclear coupling vectors, thus the COLOC experiment should be a close analog to the HETRES experiment. Since the experiment is heteronuclear, with the X spin representing the ^{13}C, and we are only interested in the proton portion of the spectrum, only the AB lines from the ABX spectrum need be considered. A second simplification in this treatment is through the assumption that the $^{1}J_{CH}$ are equal for both methylene protons. This reduces the number of parameters in the calculations through degenerating the ABX spectral parameters:

$$\mathbf{D_+ = D_- = D} \qquad [4.1]$$

$$\Theta_+ = \Theta_- = \Theta \qquad [4.2]$$

where

$$\mathbf{2D = [(\omega_A - \omega_B) + J^2_{AB}]^{1/2}} \qquad [4.3]$$

and Θ is defined by the relationships:

$$\mathbf{2D\cos 2\Theta = \omega_A - \omega_B} \qquad [4.4]$$

$$\mathbf{2D\sin 2\Theta = J_{AB}} \qquad [4.5]$$

The two AB multiplets are now identical to each other, which simplifies the calculations.

The BIRD sequence acts as a ^{1}H 180° pulse for protons directly bonded to ^{13}C while it has no effect on protons bonded to ^{12}C. In the ABX system, both protons are

bonded to ^{13}C so the BIRD sequence should be transparent. Therefore the HETRES pulse sequence should be identical to the COLOC experiment, with the delay after the 180° pulse equal to $2T-\frac{1}{2}t_1+\tau$. The calculations start with the density matrix in the Hamiltonian basis, which are the energy differences between the Hamiltonian eigenstates. These energy differences correspond to the AB lines in an ABX spectrum. These are given in table 1:

Table 4.1: Energy differences corresponding to lines in an ABX spin system.

$$|\chi_1^-) = \nu_{AB} + (-J_{AB} - J_{AX})/2 - D$$

$$|\chi_1^+) = \nu_{AB} + (-J_{AB} + J_{AX})/2 - D$$

$$|\chi_2^-) = \nu_{AB} + (J_{AB} - J_{AX})/2 - D$$

$$|\chi_2^+) = \nu_{AB} + (J_{AB} + J_{AX})/2 - D$$

$$|\chi_3^-) = \nu_{AB} + (-J_{AB} - J_{AX})/2 + D$$

$$|\chi_3^+) = \nu_{AB} + (-J_{AB} + J_{AX})/2 + D$$

$$|\chi_4^-) = \nu_{AB} + (J_{AB} - J_{AX})/2 + D$$

$$|\chi_4^+) = \nu_{AB} + (J_{AB} + J_{AX})/2 + D$$

The + and - superscripts in the density matrix elements indicate counterrotating magnetizations, and ν_{AB} represents the average frequency of the AB portion of the spectrum i.e. $(\nu_A + \nu_B)/2$.

The initial 90° pulse creates magnetizations in the xy plane which then evolve at their characteristic frequency. The pulse creates both counterrotating frequency elements, however only the evolution of the +ve elements will be followed. The density matrix elements are the $|\chi_i^+)$, and the initial 90° pulse gives magnetizations which are

proportional to the Liouville space projections of the $|\chi_i)$ along the total xy magnetization, i.e. the dot product of the density matrix element on the Liouville operator. The magnetizations right after the pulse are:

$$(\rho(0)^+|\chi_1^+) = \cos\Theta - \sin\Theta \quad [4.6]$$

$$(\rho(0)^+|\chi_2^+) = \cos\Theta + \sin\Theta \quad [4.7]$$

$$(\rho(0)^+|\chi_3^+) = \cos\Theta + \sin\Theta \quad [4.8]$$

$$(\rho(0)^+|\chi_4^+) = \cos\Theta - \sin\Theta \quad [4.9]$$

The superscript over the density matrix elements indicate that this value of the density matrix occurs immediately after the pulse, and the value in parentheses is the time index of the pulse sequence.

The magnetizations are allowed to evolve for a time $t_1/2$. This evolution is equivalent to multiplying each element in the Hamiltonian basis by e^{ivt} where:

$$\nu = |\chi_i^+) = \nu_{AB} + (\pm J_{AB} + J_{AX}) \pm D$$

and

$$t = t_1/2.$$

At this time the density matrix elements are given by the equations:

$$(\rho(\tfrac{t_1}{2})^-|\chi_1^+) = (\cos\theta - \sin\theta)e^{2\pi i(\nu_{AB}+\frac{1}{2}(-J_{AB}+J_{AX})-D)(\frac{t_1}{2})} \quad [4.10]$$

$$(\rho(\tfrac{t_1}{2})^-|\chi_2^+) = (\cos\theta + \sin\theta)e^{2\pi i(\nu_{AB}+\frac{1}{2}(J_{AB}+J_{AX})-D)(\frac{t_1}{2})} \quad [4.11]$$

$$(\rho(\tfrac{t_1}{2})^-|\chi_3^+) = (\cos\theta + \sin\theta)e^{2\pi i(\nu_{AB}+\frac{1}{2}(-J_{AB}+J_{AX})+D)(\frac{t_1}{2})} \quad [4.12]$$

$$(\rho(\tfrac{t_1}{2})^-|\chi_4^+) = (\cos\theta - \sin\theta)e^{2\pi i(\nu_{AB}+\frac{1}{2}(J_{AB}+J_{AX})+D)(\frac{t_1}{2})} \quad [4.13]$$

The effect of the 180° pulse after $t_1/2$ is to transfer each of the xy magnetizations into its counterrotating component. The effect of the pulse can be determined by converting the density matrix to the spherical tensor basis, then multiplying the density matrix by the corresponding Wigner matrix, and then transforming back to the Hamiltonian basis. In order to convert the density matrix from Hamiltonian to Liouville basis, a unitary transformation is defined which takes the superspin elements with +1 coherence into normalized transitions.

$$\begin{pmatrix} |\chi_1^+) \\ |\chi_2^+) \\ |\chi_3^+) \\ |\chi_4^+) \end{pmatrix} = U \begin{pmatrix} |1^S_{+1},1) \\ |1^A_{+1},1) \\ |1_{+1},2) \\ |2_{+1},2) \end{pmatrix} \qquad \textbf{[4.14]}$$

These normalized transitions can be converted back to superspin formation using the inverse of U ie U^{-1}. The effect of a pulse on the system can be described by a matrix, P, which transforms the magnetizations onto the various superspin basis components. The full effect of the pulse is given by the appropriate components of the Wigner matrices, $d^M(\theta)$. Since this pulse transforms all of the +1 components into -1 components, the matrix is as follows:

$$P = \begin{pmatrix} d^{1_{1-1}}(\pi) & 0 & 0 & 0 \\ 0 & d^{1_{1-1}}(\pi) & 0 & 0 \\ 0 & 0 & d^{1_{1-1}}(\pi) & 0 \\ 0 & 0 & 0 & d^{2_{1-1}}(\pi) \end{pmatrix} = \begin{pmatrix} 1 & 0 & 0 & 0 \\ 0 & 1 & 0 & 0 \\ 0 & 0 & 1 & 0 \\ 0 & 0 & 0 & 1 \end{pmatrix} \qquad \textbf{[4.15]}$$

To follow the evolution after the pulse, the density matrix is transformed back to the Hamiltonian basis. Since the pulse has transferred the xy magnetizations to their counterrotating elements, the transformation back to the Hamiltonian will be different, i.e.

$$\begin{pmatrix} |\chi_1^-) \\ |\chi_2^-) \\ |\chi_3^-) \\ |\chi_4^-) \end{pmatrix} = V \begin{pmatrix} |1^S_{-1},1) \\ |1^A_{-1},1) \\ |1_{-1},2) \\ |2_{-1},2) \end{pmatrix} \qquad \textbf{[4.16]}$$

Solving these equations yields the transformation matrices:

$$U = \frac{1}{2}\begin{pmatrix} c-s & -c-s & c+s & -c+s \\ c+s & -c+s & -c+s & c+s \\ c+s & c-s & -c+s & -c-s \\ c-s & c+s & c+s & c-s \end{pmatrix} \qquad \textbf{[4.17]}$$

$$V = \frac{1}{2}\begin{pmatrix} c-s & -c-s & -c-s & -c+s \\ c+s & -c+s & c-s & c+s \\ c+s & c-s & c-s & -c-s \\ c-s & c+s & -c-s & c-s \end{pmatrix} \qquad \textbf{[4.18]}$$

Where c = cosΘ; s = sinΘ. Since these matrices are unitary and real, their inverses are simply their transpose, i.e.

$$U^{-1} = \frac{1}{2}\begin{pmatrix} c-s & c+s & c+s & c-s \\ -c-s & -c+s & c-s & c+s \\ c+s & -c+s & -c+s & c+s \\ -c+s & c+s & -c-s & c-s \end{pmatrix} \qquad \textbf{[4.19]}$$

In order to find the value of the density matrix after the 180° pulse, the density matrix from before the pulse is left multiplied by the transformation matrix U^{-1}, then this result is left multiplied by the pulse matrix, P, and the result of this is left multiplied by V. This conversion between the +1 density matrix elements and the -1 elements through the 180°pulse becomes:

$$\begin{pmatrix} (\rho(\frac{t_1}{2})^+|\chi_1^-) \\ (\rho(\frac{t_1}{2})^+|\chi_2^-) \\ (\rho(\frac{t_1}{2})^+|\chi_3^-) \\ (\rho(\frac{t_1}{2})^+|\chi_4^-) \end{pmatrix} = VPU^{-1} \begin{pmatrix} (\rho(\frac{t_1}{2})^-|\chi_1^+) \\ (\rho(\frac{t_1}{2})^-|\chi_2^+) \\ (\rho(\frac{t_1}{2})^-|\chi_3^+) \\ (\rho(\frac{t_1}{2})^-|\chi_4^+) \end{pmatrix} \qquad [4.20]$$

The matrices VPU^{-1} can be reduced to a single matrix, P′:

$$P' = \begin{pmatrix} 0 & \cos2\Theta & 0 & -\sin2\Theta \\ \cos2\Theta & 0 & \sin2\Theta & 0 \\ 0 & \sin2\Theta & 0 & \cos2\Theta \\ -\sin2\Theta & 0 & \cos2\Theta & 0 \end{pmatrix} \qquad [4.21]$$

Thus the value of the density matrix is:

$$\begin{aligned} (\rho(\tfrac{t_1}{2})^+|\chi_1^-) &= \cos2\Theta(\cos\Theta+\sin\Theta)e^{2\pi i(\nu_{AB}+\frac{1}{2}(J_{AB}+J_{AX})-D)(\frac{t_1}{2})} \\ &\quad - \sin2\Theta(\cos\Theta-\sin\Theta)e^{2\pi i(\nu_{AB}+\frac{1}{2}(J_{AB}+J_{AX})+D)(\frac{t_1}{2})} \end{aligned} \qquad [4.22]$$

$$\begin{aligned} (\rho(\tfrac{t_1}{2})^+|\chi_2^-) &= \cos2\Theta(\cos\Theta-\sin\Theta)e^{2\pi i(\nu_{AB}+\frac{1}{2}(-J_{AB}+J_{AX})-D)(\frac{t_1}{2})} \\ &\quad + \sin2\Theta(\cos\Theta+\sin\Theta)e^{2\pi i(\nu_{AB}+\frac{1}{2}(-J_{AB}+J_{AX})+D)(\frac{t_1}{2})} \end{aligned}$$

$$(\rho(\tfrac{t_1}{2})^+|\chi_3^-) = \sin 2\Theta(\cos\Theta+\sin\Theta)e^{2\pi i(\nu_{AB}+\frac{1}{2}(J_{AB}+J_{AX})-D)(\frac{t_1}{2})} + \cos 2\Theta(\cos\Theta-\sin\Theta)e^{2\pi i(\nu_{AB}+\frac{1}{2}(J_{AB}+J_{AX})+D)(\frac{t_1}{2})} \quad [4.24]$$

$$(\rho(\tfrac{t_1}{2})^+|\chi_4^-) = -\sin 2\Theta(\cos\Theta-\sin\Theta)e^{2\pi i(\nu_{AB}+\frac{1}{2}(-J_{AB}+J_{AX})-D)(\frac{t_1}{2})} + \cos 2\Theta(\cos\Theta+\sin\Theta)e^{2\pi i(\nu_{AB}+\frac{1}{2}(-J_{AB}+J_{AX})+D)(\frac{t_1}{2})} \quad [4.25]$$

The magnetizations will then precess in the -1 direction for a time $2T - t_1/2 + \tau$, which is represented by a multiplication of each of the density matrix elements by a factor of $e^{-2\pi i\nu t}$ where $t = 2T-t_1/2+\tau$ and the ν are the $|\chi_i^-)$.

The final 90° pulse transfers ^1H polarization to the ^{13}C domain, and the final delay, Δ, is chosen so that the FID can be acquired with broadband ^1H - ^{13}C decoupling. Before the 90° pulse the proton lines are in the same form as they would be at the time of acquisition, the final 90° pulse and Δ delay merely prepare the proton lines for indirect acquisition in the carbon domain. Thus it is not necessary to follow through the calculations further. The intensities of the ^1H lines are the projection of the density matrix elements on the total xy magnetization.[40] Since the spherical tensor $|1^S_{+1},1)$ represents the total xy magnetization, the intensity is the dot product of the density matrix with this spherical tensor. The coefficients for this product are the elements in the first column of the transformation matrix, U. The resultant in this experiment will be all terms which have an exponential that has a t_1 component. This represents a modulation in t_1, which will present itself as an intensity in f_1 upon Fourier transformation in the second dimension. Simplifying the equations for the Hamiltonian terms reveals that each term

has a component with an exponential in t_1. Collecting all terms with respect to the different frequencies in t_1 shows that there are three lines, one each at $\nu_{AB} \pm D$ which are expected in the decoupled spectrum, and another at ν_{AB}. This extra line is the artifact line, appearing at the average frequency of the two methylene proton frequencies. The intensity of this line varies with the difference in chemical shift of the methylene protons and the functional form of this line is described by the non-exponential coefficients:

$$I(\nu_{AB}) = 2\sin 2\Theta\,(\sin 2\Theta \cos\tfrac{JT}{2}\cos DT + \sin\tfrac{JT}{2}\sin DT) \qquad [4.26]$$

where T is the total time of the experiment up to polarization transfer, $2T + \tau$. From this equation it can be seen that the intensity of the artifact has an oscillatory dependence on the chemical shift difference, through the D term, and an oscillatory dependence on the total time T. The equation also shows that in the limit of weak coupling, $\Theta = 0$, and the artifact intensity will also vanish.

The origin of the artifact can be rationalized through a qualitative analysis of the ABX system. In the heteronuclear ABX system, with X representing the ^{13}C, the proton spectrum is made up of two AB sub-spectra, each one a ^{13}C satellite of the uncoupled proton spectrum. In the weak coupling limit, the proton spectra would consist of two doublets, one corresponding to the A protons and the other corresponding to the B. As the strength of the coupling increases, the distinction between pure A and pure B lines can no longer be made, each line having some character of each of the nuclei. During the COLOC experiment, the coherence evolves during the first half of the experiment, and then the 180° pulse transfers coherence to those with the opposite sense of precession.

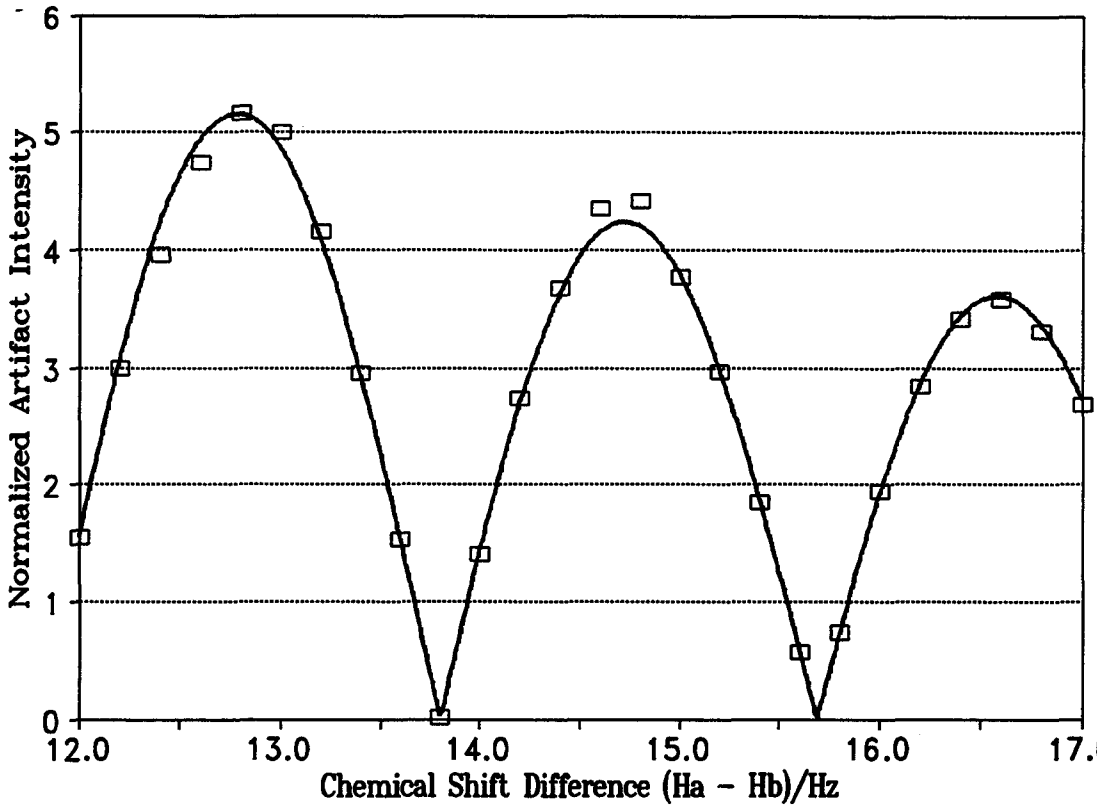

Figure 4.2: Plot of functional form for COLOC artifact intensity (solid line) compared with simulated data (boxes).

In the weak coupled case, this is simply a transfer of coherence from an A line to the corresponding B line. In the strong coupled case, each line has characteristics of both A and B spins, and this mixing will create new terms, which manifest themselves at the average of the A and B frequencies. Since this new term is made up of contributions from both A and B resonances, the intensity of the new line will be dependent on the nature of the interference between the terms, which is dependent on the chemical shift difference between the protons, and the total evolution time before polarization transfer. This new line will become coded onto the carbon coherence at polarization transfer and will be detected as a proton signal in t_1.

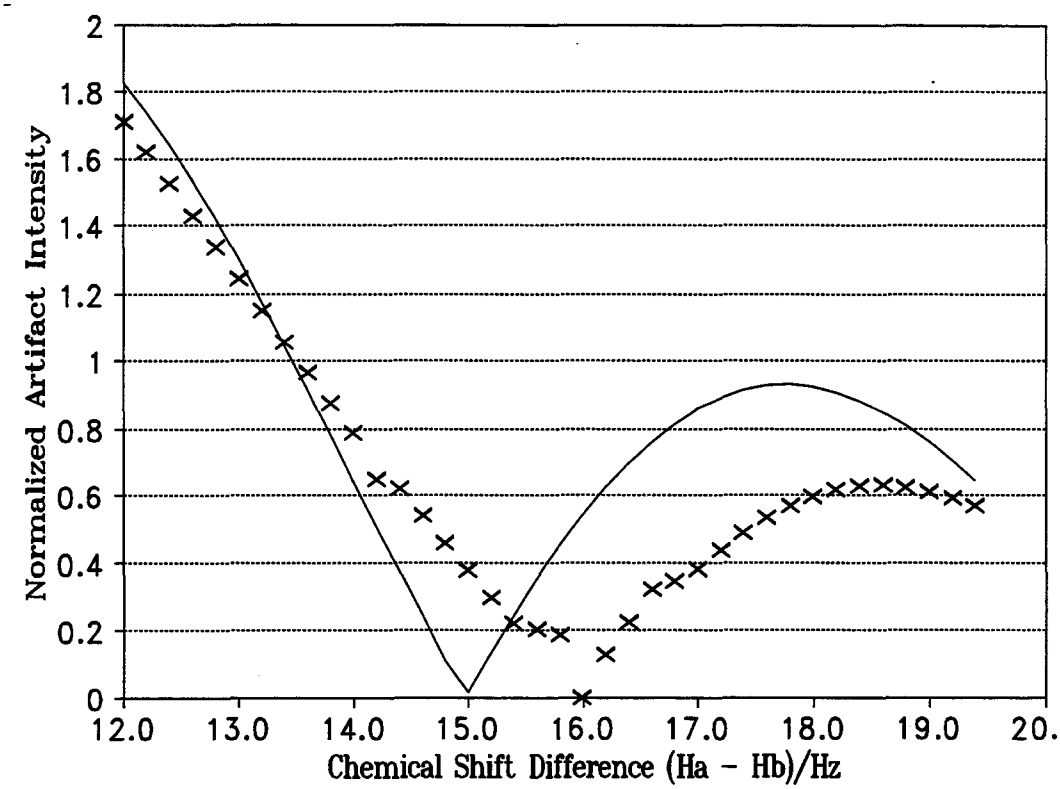

Figure 4.3: Comparison of functional form of COLOC artifact intensity (solid line) and simulated HETRES artifact intensity (X).

The analogy between the COLOC and HETRES experiments is illustrated through simulations of the two experiments. The effect of the BIRD pulse should be negligible in this case, which is supported by the comparison of the results from the simulations in figure 4.3.

In the calculations on the COLOC experiment, the system was simplified by assuming that $J_{AX} = J_{BX}$. When this assumption is relaxed, the simulations showed a splitting of the artifact. This can be rationalized by considering the effects of the assumption. When $J_{AX} = J_{BX}$, $D_+ = D_-$. The appearance of the artifact was rationalized through an argument which used D to determine the position of the artifact. When the

assumption is relaxed, there will be difference terms that will now depend on D_+ and D_-, resulting in an artifact that is split by $|D_+ - D_-|$, centred at the average value of the proton resonances.

Chapter 5

Conclusions

During the course of this thesis, the superspin formalism was used to follow the course of magnetizations through various pulse sequences for several spin systems. The advantage of using a formalism such as this is that a pulse can be visualized as a rotation of the basis in a spherical tensor basis. In addition, the general time evolution of the spherical tensors was determined for the AX, AX_2, and AX_3 systems, which meant that it was not necessary to change to the Hamiltonian basis during a time evolution. These general evolution equations can be used in the analysis of other pulse sequences, although for the AX_2 and AX_3 systems this would be better done by computer than by hand. Another advantage of studying a pulse sequence in this manner is that the evolution of the coherences can be studied in detail at each step of the pulse sequence.

The general evolution equations were initially tested using simpler pulse sequences than were demonstrated in this thesis. Each set of general evolution equations was tested using the ^{1}H and ^{13}C single pulse experiments and the DEPT experiment. In each system

the one pulse experiments yielded the correct number of lines, and the DEPT experiment showed the correct θ pulse dependence for each of the spin systems. These results increased the confidence that the general evolution equations were correct, however the BIRD study provided a more robust verification of this. Despite all of the verifications using simpler pulse sequences, a functional form for the intensity of the carbon signal in the AX_3 system could not be derived by hand, due to the large number of equations involved. To further this study, this functional form for the AX_3 system under the INEPT-BIRD sequence could be derived with the aid of computer aided symbolic math programs (such as Maple). The graphical form of the AX_3 system was derived using the simulation program SIMPLTN[53] which gave enough data to illustrate and discuss the trends through the AX, AX_2 and AX_3 systems. It is also possible that SIMPLTN could be used in the future to help elucidate the functional form of the AX_3 system.

The BIRD pulse sequence has been shown to exhibit anomalous behaviour which is dependent upon the interpulse delay. In the preceding analysis, the BIRD pulse was applied to a system where polarization had been transferred from protons to carbons, leaving the protons with zero coherence. The initial 90° pulse in the BIRD sequence will then create carbon-proton multiple quantum coherence. In general, a 90° pulse applied to any non-equilibrium spin system will create multiple quantum coherence, the levels being determined by the element of the Wigner rotation matrix for that system. The BIRD pulse should refocus all coherence back to the carbon domain to be detected. This is successful due to the symmetry of the BIRD sequence about the 180° pulse and the selection of the interpulse delay. Thus any coherence that evolves during the first delay

will be refocussed during the second delay after the 180° pulses. In a simple AX system, the amount of carbon coherence will be maximized when the value of the interpulse delay is $1/J_{AX}$, with the intensity varying sinusoidally as the delay is varied. In the AX system the multiple quantum levels do not play any part in the intensity of the final signal. In higher order systems, such as AX_2 and AX_3 systems, there are multiple quantum levels which are accessed through the initial 90° pulse, which do not evolve at the same rate as the single quantum coherence. Thus as the delays are varied, the intensity of the detected carbon signal will also depend on the evolution of multiple quantum levels. In the AX_2 system, there is an additional dependence which varies at twice the frequency of the single quantum level, and in the AX_3 system there is an additional dependence which has three times the frequency. The variations of intensity for the AX, AX_2, and AX_3 systems was illustrated in chapter 3.

This study of BIRD pulses has helped to show in greater detail, the effects of multiple pulses on complex spin systems. In the BIRD study it was shown that the description of the effect of the BIRD pulse based on the most simple spin system is only correct in a general sense. When more complex systems are studied in detail it was shown that multiple quantum levels are created and that they contribute to the intensity of the detected signal. It was also shown how the phase cycle of the final 90° pulse is manifested as a shift in phase with respect to the BIRD delay. At delays corresponding to the maxima and null of the carbon line the signal intensity is predicted by the vector model, however this model fails to predict the behaviour at delay times which are not integral multiples of the coupling constant, or when the pulse phases differ from multiples

of 90°. This is where the Superspin formalism has its advantages. With the functional form which is derived from using this formalism, the effect of combining phase cycles can be visualized. This led to the hypothesis that with the correct combination of phase cycles, that BIRD pulses could be used for spectral editing in AX, AX_2 and AX_3 systems. This remains a topic for further study, both as a theoretical analysis and in the development of practical applications.

The analysis of artifacts in two dimensional NMR spectra can be used to learn about the effects of a pulse sequence on a spin system. In chapter 4 of this thesis, an artifact that arose in a methylene group was used to study constant evolution time pulse sequences. Through the course of the analysis of the pulse sequence, it can be seen how the coupling constant dependence of the magnetizations is cancelled out after the 180° pulses transfer coherences to their counter-rotating elements. In this type of experiment the artifact line is obvious as the only term which does not correspond to one of the two frequencies of the A or B protons. The analysis of the COLOC and HETRES experiments showed the similarity between these two experiments, and that the effect of the BIRD sequence, provided that the parameters have been set properly, has little effect on the appearance of the artifact. Deriving a functional form for the intensities of the lines in the spectra also helps rationalize the behaviour of the artifact, in the present case it illustrated the dependence of the artifacts intensity on the difference in the chemical shift. The overall dependence of the artifact intensity on the strength of the coupling was also shown. The intensity of the artifact was attenuated proportional to the strength of the coupling. In the limit of weak coupling there is no artifact because the lines

corresponding to the A and B spins are distinct, and there will be a clean transfer of coherence between the A lines and the B lines by the 180° pulse in the COLOC experiment. The analysis of artifacts in this manner shows the origin of the artifact, and whether the artifact is persistent or can be minimized through creative use of phase cycling. In this case the artifact was found to be persistent. Using the formalisms introduced in this study, different phase cycles can be investigated with respect to the artifact. This has implications from an experimental viewpoint in that suspect peaks in a spectrum can be assigned as artifacts through studies such as these, or using computer simulations based on this formalism.

Appendix 1

Energy Level Diagrams for the AX, AX_2 and AX_3 Systems

Energy Level Diagram for AX System

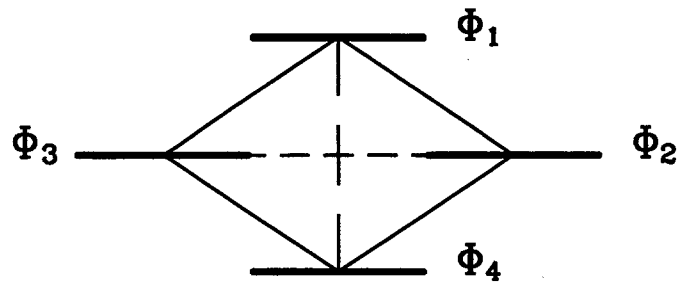

——— Single Quantum Transition
— —— — Double Quantum Transition
- — — — - Zero Quantum Transition

Energy Level Diagram For AX_2 System

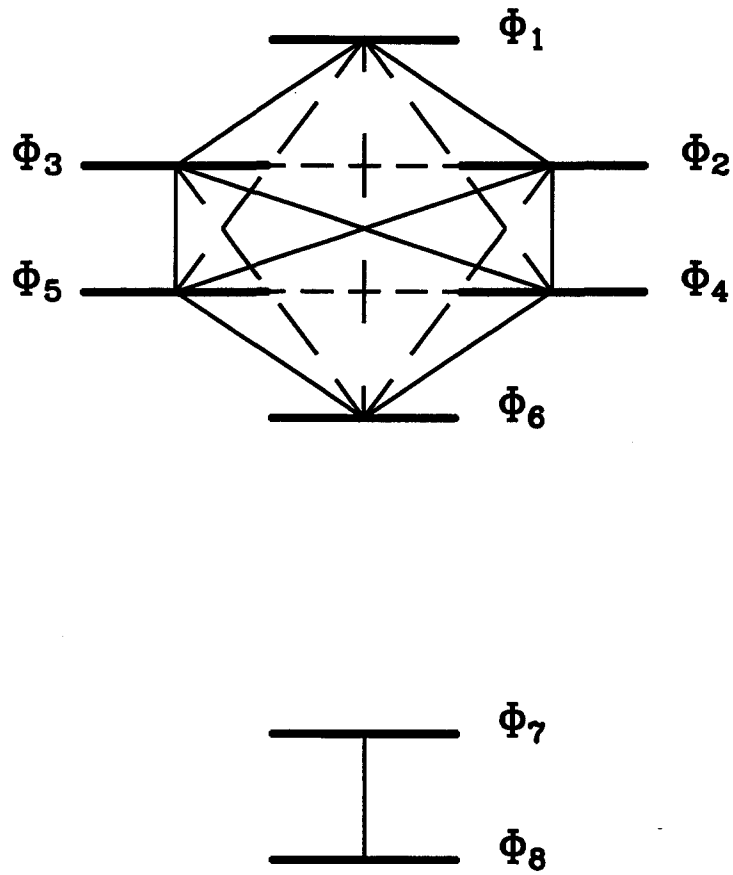

——— Single Quantum Transition
— —— — Double Quantum Transition
- — — — - Zero Quantum Transition
—— —— Triple Quantum Transition

Energy Level Diagram for AX_3 System

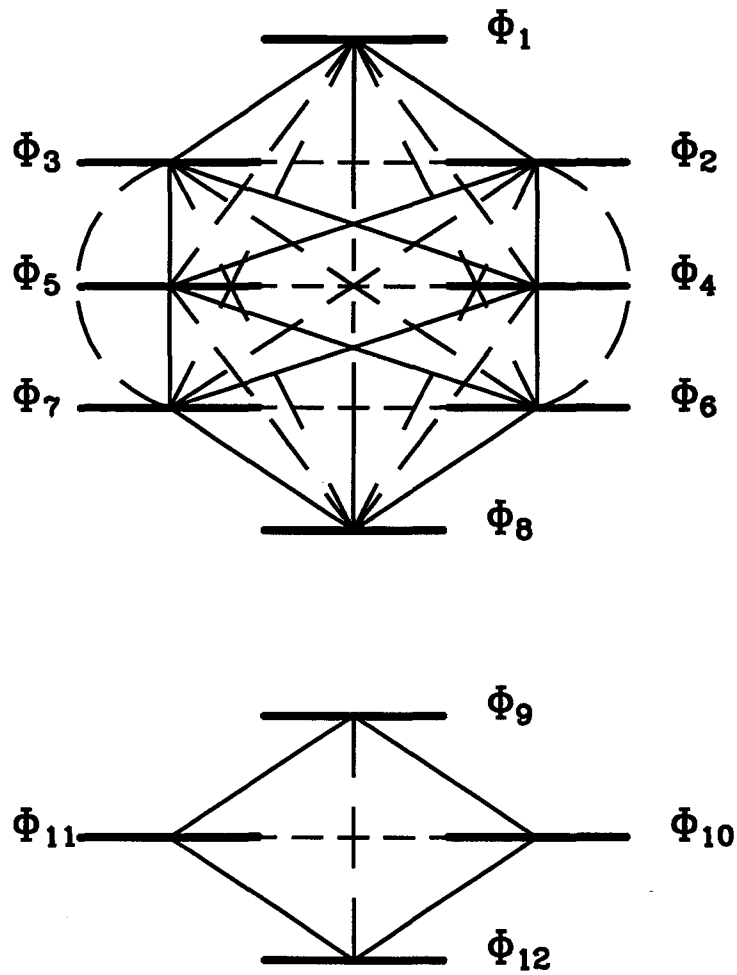

Appendix 2

Spherical Tensor Basis for Two and Three Coupled Spins 1/2

in Terms of Single Spin Basis Vectors

Spherical Tensor Basis for Two Coupled Spins 1/2

$$|0,0) = |0)|0)$$

$$|0,2) = \frac{1}{\sqrt{3}}\{|1_{+1})|1_{-1}) + |1_{-1})|1_{+1}) - |1_0)|1_0)\}$$

$$|1^S_{+1},1) = \frac{1}{\sqrt{2}}\{|1_{+1})|0) + |0)|1_{+1})\}$$

$$|1^S_0,1) = \frac{1}{\sqrt{2}}\{|1_0)|0) + |0)|1_0)\}$$

$$|1^S_{-1},1) = \frac{1}{2}\{|1_{-1})|0) + |0)|1_{-1})\}$$

$$|2_{+2},2) = |1_{+1})|1_{+1})$$

$$|2_{+1},2) = \frac{1}{\sqrt{2}}\{|1_{+1})|1_0) + |1_0)|1_{+1})\}$$

$$|2_0,2) = \frac{1}{\sqrt{6}}\{|1_{+1})|1_{-1}) + |1_{-1})|1_{+1}) + 2|1_0)|1_0)\}$$

$$|2_{-1},2) = \frac{1}{\sqrt{2}}\{|1_{-1})|1_0) + |1_0)|1_{-1})\}$$

$$|2_{-2},2) = |1_{-1})|1_{-1})$$

Spherical Tensor Basis for Three Coupled Spins 1/2

$$|0,0) = |0)|0)|0)$$

$$\begin{aligned}|0,2) = \tfrac{1}{3}\{&|1_{+1})|1_{-1})|0) + |1_{-1})|1_{+1})|0) + |1_{-1})|0)|1_{+1}) \\ &+ |1_{+1})|0)|1_{-1}) + |0)|1_{+1})|_{-1}) + |0)|1_{-1})|1_{+1}) \\ &- |0)|1_0)|1_0) - |1_0)|0)|1_0) - |1_0)|1_0)|0)\}\end{aligned}$$

$$|1_0,1) = \frac{1}{\sqrt{3}}\{|1_0)|0)|0) + |0)|1_0)|0) + |0)|0)|1_0)\}$$

$$\begin{aligned}|1_0,3) = \frac{1}{\sqrt{3}\sqrt{5}}\{&|1_{+1})|1_{-1})|1_0) + |1_{+1})|1_0)|1_{-1}) + |1_0)|1_{+1})|1_{-1}) \\ &+ |1_{-1})|1_{+1})|1_0) + |1_{-1})|1_0)|1_{+1}) + |1_0)|1_{-1})|1_{+1})\} \\ &- \frac{\sqrt{3}}{\sqrt{5}}|1_0)|1_0)|1_0)\end{aligned}$$

$$\begin{aligned}|2_0,2) = \frac{1}{3\sqrt{2}}\{&|1_{+1})|1_{-1})|0) + |1_{+1})|0)|1_{-1}) + |0)|_{+1})|_{-1}) \\ &+ |_{-1})|_{+1})|0) + |1_{-1})|0)|_{+1}) + |0)|1_{-1})|1_{+1})\} \\ &+ \frac{2}{3\sqrt{2}}\{|1_0)|1_0)|0) + |1_0)|0)|1_0) + |0)|1_0)|1_0)\}\end{aligned}$$

$$\begin{aligned}|3_0,3) = \frac{1}{\sqrt{2}\sqrt{5}}\{&|1_{+1})|1_{-1})|1_0) + |1_{+1})|_0)|_{-1}) + |_0)|_{+1})|_{-1}) \\ &+ |1_{-1})|1_{+1})|1_0) + |1_{-1})|1_0)|1_{+1}) + |1_0)|1_{-1})|1_{+1})\} \\ &- \frac{\sqrt{2}}{\sqrt{5}}|1_0)|1_0)|1_0)\end{aligned}$$

$$|1_{+1},1) = \frac{1}{\sqrt{3}}\{|1_{+1})|0)|0) + |0)|1_{+1})|0) + |0)|0)|1_{+1})\}$$

$$|3_{+1},3) = \frac{2}{\sqrt{3}\sqrt{5}}\{|1_{+1})|1_0)|1_0) + |1_0)|1_{+1}|1_0) + |1_0)|1_0)|1_{+1})\}$$
$$+ \frac{1}{\sqrt{3}\sqrt{5}}\{|1_{+1})|1_{+1})|1_{-1}) + |1_{+1})|1_{-1})|1_{+1}) + |1_{-1})|1_{+1})|1_{+1})\}$$

$$|2_{+1},2) = \frac{1}{\sqrt{6}}\{|1_{+1})|1_0)|0) + |1_{+1})|0)|1_0) + |0)|1_{+1})|1_0)$$
$$+ |1_0)|_{+1})|0) + |1_0)|0)|1_{+1}) + |0)|1_0)|_{+1})\}$$

$$|1_{+1},3) = -\frac{1}{\sqrt{3}\sqrt{5}}\{|1_{+1})|1_0)|1_0) + |1_0)|1_{+1})|1_0) + |1_0)|1_0)|1_{+1})\}$$
$$+ \frac{2}{\sqrt{3}\sqrt{5}}\{|1_{+1})|1_{+1})|1_{-1}) + |1_{+1})|1_{-1})|1_{+1}) + |1_{-1})|1_{+1})|1_{+1})\}$$

$$|1_{-1},1) = \frac{1}{\sqrt{3}}\{|1_{-1})|0)|0)+|0)|1_{-1})|0) + |0)|0)|1_{-1})\}$$

$$|3_{-1},3) = \frac{2}{\sqrt{3}\sqrt{5}}\{|1_{-1})|1_0)|1_0) + |1_0)|1_{-1}|1_0) + |1_0)|1_0)|1_{-1})\}$$
$$+ \frac{1}{\sqrt{3}\sqrt{5}}\{|1_{-1})|1_{-1})|1_{+1}) + |1_{-1})|1_{+1})|1_{-1}) + |1_{+1})|1_{-1})|1_{-1})\}$$

$$|2_{-1},2) = \frac{1}{\sqrt{6}}\{|1_{-1})|1_0)|0) + |1_{-1})|0)|1_0) + |0)|1_{-1})|1_0)$$
$$+ |1_0)|_{-1})|0) + |1_0)|0)|1_{-1}) + |0)|1_0)|_{-1})\}$$

$$|1_{-1},3) = -\frac{1}{\sqrt{3}\sqrt{5}}\{|1_{-1})|1_0)|1_0) + |1_0)|1_{-1})|1_0) + |1_0)|1_0)|1_{-1})\}$$
$$+ \frac{2}{\sqrt{3}\sqrt{5}}\{|1_{-1})|1_{-1})|1_{+1}) + |1_{-1})|1_{+1})|1_{-1}) + |1_{+1})|1_{-1})|1_{-1})\}$$

$$|2_{+2},2) = \frac{1}{\sqrt{3}}\{|1_{+1})|1_{+1})|0) + |1_{+1})|0)|_{+1}) + |0)|1_{+1}|1_{+1})\}$$

$$|3_{+2},3) = \frac{1}{\sqrt{3}}\{|1_{+1})|1_{+1})|1_0) + |1_{+1})|1_0)|1_{+1}) + |1_0)|1_{+1})|1_{+1})\}$$

$$|2_{-2},2) = \frac{1}{\sqrt{3}}\{|1_{-1})|1_{-1})|0) + |1_{-1})|0)|_{-1}) + |0)|1_{-1})|_{-1})\}$$

$$|3_{-2},3) = \frac{1}{\sqrt{3}}\{|1_{-1})|1_{-1})|1_0) + |1_{-1})|1_0)|_{-1}) + |1_0)|1_{-1})|1_{-1})\}$$

$$|3_{+3},3) = |1_{+1})|1_{+1})|1_{+1})$$

$$|3_{-3},3) = |1_{-1})|1_{-1})|1_{-1})$$

Appendix 3

Tables of General Evolution of the

Spherical Tensors for the AX, AX_2, and AX_3 Systems

General Evolution of the

Spherical Tensors for the AX System

Single Quantum Transitions

$$|0\rangle|1_{+1}\rangle = e^{i\nu_X t}\cos\frac{Jt}{2}|0\rangle|1_{+1}\rangle + ie^{i\nu_X t}\sin\frac{Jt}{2}|1_0\rangle|1_{+1}\rangle$$

$$|1_0\rangle|1_{+1}\rangle = ie^{i\nu_X t}\sin\frac{Jt}{2}|0\rangle|1_{+1}\rangle + e^{i\nu_X t}\cos\frac{Jt}{2}|1_0\rangle|1_{+1}\rangle$$

$$|0\rangle|1_{-1}\rangle = e^{-i\nu_X t}\cos\frac{Jt}{2}|0\rangle|1_{-1}\rangle - ie^{-i\nu_X t}\sin\frac{Jt}{2}|1_0\rangle|1_{-1}\rangle$$

$$|1_0\rangle|1_{-1}\rangle = -ie^{-i\nu_X t}\sin\frac{Jt}{2}|0\rangle|1_{-1}\rangle + e^{i\nu_X t}\cos\frac{Jt}{2}|1_0\rangle|1_{-1}\rangle$$

$$|1_{+1}\rangle|0\rangle = e^{i\nu_A t}\cos\frac{Jt}{2}|1_{+1}\rangle|0\rangle + ie^{i\nu_A t}\sin\frac{Jt}{2}|1_{+1}\rangle|1_0\rangle$$

$$|1_{+1}\rangle|1_0\rangle = ie^{i\nu_A t}\sin\frac{Jt}{2}|1_{+1}\rangle|0\rangle + e^{i\nu_A t}\cos\frac{Jt}{2}|1_{+1}\rangle|1_0\rangle$$

$$|1_{-1}\rangle|0\rangle = e^{i\nu_A t}\cos\frac{Jt}{2}|1_{-1}\rangle|0\rangle - ie^{i\nu_A t}\sin\frac{Jt}{2}|1_{-1}\rangle|1_0\rangle$$

$$|1_{-1}\rangle|1_0\rangle = -ie^{i\nu_A t}\sin\frac{Jt}{2}|1_{-1}\rangle|0\rangle + e^{i\nu_A t}\cos\frac{Jt}{2}|1_{-1}\rangle|1_0\rangle$$

Zero-Quantum Transitions

$$|1_{+1}\rangle|1_{-1}\rangle = e^{i(\nu_A-\nu_X)t}|1_{+1}\rangle|1_{-1}\rangle$$

$$|1_{-1}\rangle|1_{+1}\rangle = e^{-i(\nu_A-\nu_X)t}|1_{-1}\rangle|1_{+1}\rangle$$

Double Quantum Transitions

$$|1_{+1}\rangle|1_{+1}\rangle = e^{i(\nu_A+\nu_X)t}|1_{+1}\rangle|1_{+1}\rangle$$

$$|1_{-1}\rangle|1_{-1}\rangle = e^{-i(\nu_A+\nu_X)t}|1_{-1}\rangle|1_{-1}\rangle$$

General Evolution of the

Spherical Tensors for the AX_2 System

Single Quantum Transitions

$$|0\rangle|1_{-1},1\rangle = e^{-iv_x t}[\cos(\tfrac{1}{2}Jt)|0\rangle|1_{-1},1\rangle - i\sin(\tfrac{1}{2}Jt)|1_0\rangle|1_{-1},1\rangle$$

$$|0\rangle|2_{-1},2\rangle = e^{-iv_x t}[\cos(\tfrac{1}{2}Jt)|0\rangle|2_{-1},2\rangle - i\sin(\tfrac{1}{2}Jt)|1_0\rangle|2_{-1},2\rangle$$

$$|1_0\rangle|1_{-1},1\rangle = e^{-iv_x t}[-i\sin(\tfrac{1}{2}Jt)|0\rangle|1_{-1},1\rangle + \cos(\tfrac{1}{2}Jt)|1_0\rangle|1_{-1},1\rangle$$

$$|1_0\rangle|2_{-1},2\rangle = e^{-iv_x t}[-i\sin(\tfrac{1}{2}Jt)|0\rangle|2_{-1},2\rangle + \cos(\tfrac{1}{2}Jt)|1_0\rangle|2_{-1},2\rangle$$

$$|0\rangle|1_{+1},1\rangle = e^{iv_x t}[\cos(\tfrac{1}{2}Jt)|0\rangle|1_{+1},1\rangle + i\sin(\tfrac{1}{2}Jt)|1_0\rangle|1_{+1},1\rangle$$

$$|0\rangle|2_{+1},2\rangle = e^{iv_x t}[\cos(\tfrac{1}{2}Jt)|0\rangle|2_{+1},2\rangle + i\sin(\tfrac{1}{2}Jt)|1_0\rangle|2_{+1},2\rangle]$$

$$|1_0\rangle|1_{+1},1\rangle = e^{iv_x t}[i\sin(\tfrac{1}{2}Jt)|0\rangle|1_{+1},1\rangle + i\cos(\tfrac{1}{2}Jt)|1_0\rangle|1_{+1},1\rangle$$

$$|1_0\rangle|2_{+1},2\rangle = e^{iv_x t}[i\sin(\tfrac{1}{2}Jt)|0\rangle|2_{+1},2\rangle + \cos(\tfrac{1}{2}Jt)|1_0\rangle|2_{+1},2\rangle$$

$$|1_{+1}\rangle|0,0\rangle = e^{iv_A t}[\tfrac{1}{2}(1+\cos Jt)|1_{+1}\rangle|0,0\rangle + \tfrac{1}{\sqrt{2}}i\sin Jt|1_{+1}\rangle|1_0,1\rangle - \tfrac{1}{\sqrt{6}}(1-\cos Jt)|1_{+1}|2_0,2\rangle + \tfrac{1}{2\sqrt{3}}(1-\cos Jt)|1_{+1}\rangle|0,2\rangle]$$

$$|1_{+1}\rangle|1_0,1\rangle = e^{iv_A t}[\tfrac{1}{\sqrt{2}}i\sin Jt|1_{+1}\rangle|0,0\rangle + \cos Jt|1_{+1}\rangle|1_0,1\rangle + \tfrac{1}{\sqrt{3}}i\sin Jt|1_{+1}|2_0,2\rangle - \tfrac{1}{\sqrt{6}}i\sin Jt|1_{+1}\rangle|0,2\rangle]$$

$$|1_{+1}\rangle|0,2\rangle = e^{iv_A t}[\tfrac{1}{2\sqrt{3}}(1-\cos Jt)|1_{+1}\rangle|0,0\rangle - \tfrac{1}{\sqrt{6}}i\sin Jt|1_{+1}\rangle|1_0,1\rangle + \tfrac{1}{3\sqrt{2}}(1-\cos Jt)|1_{+1}|2_0,2\rangle + \tfrac{1}{6}(5+\cos Jt)|1_{+1}\rangle|0,2\rangle]$$

$$|1_{+1}\rangle|2_0,2\rangle = e^{iv_A t}[-\tfrac{1}{\sqrt{6}}(1-\cos Jt)|1_{+1}\rangle|0,0\rangle + \tfrac{1}{\sqrt{3}}i\sin Jt|1_{+1}\rangle|1_0,1\rangle + \tfrac{1}{3}(2+\cos Jt)|1_{+1}|2_0,2\rangle + \tfrac{1}{3\sqrt{2}}(1-\cos Jt)|1_{+1}\rangle|0,2\rangle]$$

$$|1_{-1}\rangle|0,0\rangle = e^{-iv_A t}[\tfrac{1}{2}(1+\cos Jt)|1_{-1}\rangle|0,0\rangle - \tfrac{1}{\sqrt{2}}i\sin Jt|1_{-1}\rangle|1_0,1\rangle - \tfrac{1}{\sqrt{6}}(1-\cos Jt)|1_{-1}|2_0,2\rangle + \tfrac{1}{2\sqrt{3}}(1-\cos Jt)|1_{-1}\rangle|0,2\rangle]$$

$$|1_{-1}\rangle|1_0,1\rangle = e^{-iv_A t}[-\tfrac{1}{\sqrt{2}}i\sin Jt|1_{-1}\rangle|0,0\rangle + \cos Jt|1_{-1}\rangle|1_0,1\rangle - \tfrac{1}{\sqrt{3}}i\sin Jt|1_{-1}|2_0,2\rangle + \tfrac{1}{\sqrt{6}}i\sin Jt)|1_{-1}\rangle|0,2\rangle]$$

$$|1_{-1}\rangle|2_0,2\rangle = e^{-i\nu_A t}[-\frac{1}{\sqrt{6}}(1-\cos Jt)|1_{-1}\rangle|0,0\rangle - \frac{1}{\sqrt{3}}i\sin Jt|1_{-1}\rangle|1_0,1\rangle + \frac{1}{3}(2+\cos Jt)|1_{-1}|2_0,2\rangle + \frac{1}{3\sqrt{2}}(1-\cos Jt)|1_{-1}\rangle|0,2\rangle]$$

$$|1_{-1}\rangle|0,2\rangle = e^{-i\nu_A t}[\frac{1}{2\sqrt{3}}(1-\cos Jt)|1_{-1}\rangle|0,0\rangle + \frac{1}{\sqrt{6}}i\sin Jt|1_{-1}\rangle|1_0,1\rangle + \frac{1}{3\sqrt{2}}(1-\cos Jt)|1_{-1}|2_0,2\rangle + \frac{1}{6}(5+\cos Jt)|1_{-1}\rangle|0,2\rangle]$$

$$|1_{+1}\rangle|2_{-2},2\rangle = e^{i(\nu_A-2\nu_X)t}|1_{+1}\rangle|2_{-2},2\rangle$$

$$|1_{-1}\rangle|2_{+2},2\rangle = e^{-i(\nu_A-2\nu_X)t}|1_{-1}\rangle|2_{+2},2\rangle$$

Zero Quantum Transitions

$$|1_{+1}\rangle|1_{-1},1\rangle = e^{i(\nu_A-\nu_X)t}[\cos(\tfrac{1}{2}Jt)|1_{+1}\rangle|1_{-1},1\rangle + i\sin(\tfrac{1}{2}Jt)|1_{+1}\rangle|2_{-1},2\rangle]$$

$$|1_{+1}\rangle|2_{-1},2\rangle = e^{i(\nu_A-\nu_X)t}[i\sin(\tfrac{1}{2}Jt)|1_{+1}\rangle|1_{-1},1\rangle + \cos(\tfrac{1}{2}Jt)|1_{+1}\rangle|2_{-1},2\rangle]$$

$$|1_{-1}\rangle|1_{+1},1\rangle = e^{-i(\nu_A-\nu_X)t}[\cos(\tfrac{1}{2}Jt)|1_{-1}\rangle|1_{+1},1\rangle - i\sin(\tfrac{1}{2}Jt)|1_{-1}\rangle|2_{+1},2\rangle]$$

$$|1_{-1}\rangle|2_{+1},2\rangle = e^{-i(\nu_A-\nu_X)t}[-i\sin(\tfrac{1}{2}Jt)|1_{-1}\rangle|1_{+1},1\rangle + \cos(\tfrac{1}{2}Jt)|1_{-1}\rangle|2_{+1},2\rangle]$$

Double Quantum Transitions

$$|1_{+1}\rangle|1_{+1},1\rangle = e^{i(\nu_A+\nu_X)t}[\cos(\tfrac{1}{2}Jt)|1_{+1}\rangle|1_{+1},1\rangle + i\sin(\tfrac{1}{2}Jt)|1_{+1}\rangle|2_{+1},2\rangle$$

$$|1_{+1}\rangle|2_{+1},2\rangle = e^{i(\nu_A+\nu_X)t}[i\sin(\tfrac{1}{2}Jt)|1_{+1}\rangle|1_{+1},1\rangle + \cos(\tfrac{1}{2}Jt)|1_{+1}\rangle|2_{+1},2\rangle$$

$$|1_{-1}\rangle|1_{-1},1\rangle = e^{-i(\nu_A+\nu_X)t}[\cos(\tfrac{1}{2}Jt)|1_{-1}\rangle|1_{-1},1\rangle - i\sin(\tfrac{1}{2}Jt)|1_{-1}\rangle|2_{-1},2\rangle$$

$$|1_{-1}\rangle|2_{-1},2\rangle = e^{-i(\nu_A+\nu_X)t}[-i\sin(\tfrac{1}{2}Jt)|1_{-1}\rangle|1_{-1},1\rangle + \cos(\tfrac{1}{2}Jt)|1_{-1}\rangle|2_{-1},2\rangle$$

$$|0\rangle|2_{+2},2\rangle = e^{i(2\nu_X)t}[\cos(Jt)|0\rangle|2_{+2},2\rangle + i\sin(Jt)|1_0\rangle|2_{+2},2\rangle$$

$$|1_0\rangle|2_{+2},2\rangle = e^{i(2\nu_X)t}[i\sin(Jt)|0\rangle|2_{+2},2\rangle + \cos(Jt)|1_0\rangle|2_{+2},2\rangle$$

$$|0\rangle|2_{-2},2\rangle = e^{-i(2\nu_X)t}[\cos(Jt)|0\rangle|2_{-2},2\rangle - i\sin(Jt)|1_0\rangle|2_{-2},2\rangle$$

$$|1_0\rangle|2_{-2},2\rangle = e^{-i(2\nu_X)t}[-i\sin(Jt)|0\rangle|2_{-2},2\rangle + \cos(Jt)|1_0\rangle|2_{-2},2\rangle$$

Triple Quantum Transitions

$$|1_{+1}\rangle|2_{+2},2\rangle = e^{i(\nu_A+2\nu_X)t}|1_{+1}\rangle|2_{+2},2\rangle$$

$$|1_{-1}\rangle|2_{-2},2\rangle = e^{-i(\nu_A+2\nu_X)t}|1_{-1}\rangle|2_{-2},2\rangle$$

General Evolution for Spherical Tensors

for the AX_3 Spin System

Single Quantum Transitions

$$|1_{+1}\rangle|0,0\rangle = e^{-iv_A t}[\tfrac{1}{4}(\cos\tfrac{3}{2}Jt + 3\cos\tfrac{1}{2}Jt)|1_{+1}\rangle|0,0\rangle - \tfrac{\sqrt{3}}{4}(i\sin\tfrac{3}{2}Jt + i\sin\tfrac{1}{2}Jt)|1_{+1}\rangle|1_0,1\rangle$$
$$-\tfrac{1}{4}(\cos\tfrac{3}{2}Jt - \cos\tfrac{1}{2}Jt)|1_{+1}\rangle|0,2\rangle + \tfrac{1}{2\sqrt{2}}(\cos\tfrac{3}{2}Jt - \cos\tfrac{1}{2}Jt)|1_{+1}\rangle|2_0,2\rangle$$
$$+\tfrac{\sqrt{3}}{4\sqrt{5}}(i\sin\tfrac{3}{2}Jt - 3i\sin\tfrac{1}{2}Jt)|1_{+1}\rangle|1_0,3\rangle - \tfrac{1}{2\sqrt{2}\sqrt{5}}(i\sin\tfrac{3}{2}Jt - 3i\sin\tfrac{1}{2}Jt)|1_{+1}\rangle|3_0,3\rangle]$$

$$|1_{+1}\rangle|1_0,1\rangle = e^{-iv_A t}[-\tfrac{\sqrt{3}}{4}(i\sin\tfrac{3}{2}Jt + i\sin\tfrac{1}{2}Jt)|1_{+1}\rangle|0,0\rangle + \tfrac{1}{4}(3\cos\tfrac{3}{2}Jt + \cos\tfrac{1}{2}Jt)|1_{+1}\rangle|1_0,1\rangle$$
$$+\tfrac{1}{4\sqrt{3}}(3i\sin\tfrac{3}{2}Jt - i\sin\tfrac{1}{2}Jt)|1_{+1}\rangle|0,2\rangle - \tfrac{1}{2\sqrt{6}}(3i\sin\tfrac{3}{2}Jt - i\sin\tfrac{1}{2}Jt)|1_{+1}\rangle|2_0,2\rangle$$
$$-\tfrac{3}{4\sqrt{5}}(\cos\tfrac{3}{2}Jt - \cos\tfrac{1}{2}Jt)|1_{+1}\rangle|1_0,3\rangle + \tfrac{\sqrt{3}}{2\sqrt{2}\sqrt{5}}(\cos\tfrac{3}{2}Jt - \cos\tfrac{1}{2}Jt)|1_{+1}\rangle|3_0,3\rangle]$$

$$|1_{+1}\rangle|0,2\rangle = e^{-iv_A t}[-\tfrac{1}{4}(\cos\tfrac{3}{2}Jt - \cos\tfrac{1}{2}Jt)|1_{+1}\rangle|0,0\rangle + \tfrac{1}{4\sqrt{3}}(3i\sin\tfrac{3}{2}Jt - i\sin\tfrac{1}{2}Jt)|1_{+1}\rangle|1_0,1\rangle$$
$$+\tfrac{1}{4}(\cos\tfrac{3}{2}Jt + 3\cos\tfrac{1}{2}Jt)|1_{+1}\rangle|0,2\rangle - \tfrac{1}{2\sqrt{2}}(\cos\tfrac{3}{2}Jt - \cos\tfrac{1}{2}Jt)|1_{+1}\rangle|2_0,2\rangle$$
$$-\tfrac{1}{4\sqrt{3}\sqrt{5}}(3i\sin\tfrac{3}{2}Jt + 11i\sin\tfrac{1}{2}Jt)|1_{+1}\rangle|1_0,3\rangle + \tfrac{1}{2\sqrt{2}\sqrt{5}}(i\sin\tfrac{3}{2}Jt - 3i\sin\tfrac{1}{2}Jt)|1_{+1}\rangle|3_0,3\rangle]$$

$$|1_{+1}\rangle|2_0,2\rangle = e^{-iv_A t}[\tfrac{1}{2\sqrt{2}}(\cos\tfrac{3}{2}Jt - \cos\tfrac{1}{2}Jt)|1_{+1}\rangle|0,0\rangle - \tfrac{1}{2\sqrt{6}}(3i\sin\tfrac{3}{2}Jt - i\sin\tfrac{1}{2}Jt)|1_{+1}\rangle|1_0,1\rangle$$
$$-\tfrac{1}{2\sqrt{2}}(\cos\tfrac{3}{2}Jt - \cos\tfrac{1}{2}Jt)|1_{+1}\rangle|0,2\rangle + \tfrac{1}{2}(\cos\tfrac{3}{2}Jt + \cos\tfrac{1}{2}Jt)|1_{+1}\rangle|2_0,2\rangle$$
$$+\tfrac{1}{2\sqrt{5}\sqrt{6}}(3i\sin\tfrac{3}{2}Jt - i\sin\tfrac{1}{2}Jt)|1_{+1}\rangle|1_0,3\rangle - \tfrac{1}{2\sqrt{5}}(i\sin\tfrac{3}{2}Jt + 3i\sin\tfrac{1}{2}Jt)|1_{+1}\rangle|3_0,3\rangle]$$

$$|1_{+1}\rangle|1_0,3\rangle = e^{-iv_A t}[\tfrac{\sqrt{3}}{4\sqrt{5}}(i\sin\tfrac{3}{2}Jt - 3i\sin\tfrac{1}{2}Jt)|1_{+1}\rangle|0,0\rangle - \tfrac{3}{4\sqrt{5}}(\cos\tfrac{3}{2}Jt - \cos\tfrac{1}{2}Jt)|1_{+1}\rangle|1_0,1\rangle$$
$$-\tfrac{1}{4\sqrt{5}\sqrt{3}}(3i\sin\tfrac{3}{2}Jt + 11i\sin\tfrac{1}{2}Jt)|1_{+1}\rangle|0,2\rangle + \tfrac{1}{2\sqrt{5}\sqrt{6}}(3i\sin\tfrac{3}{2}Jt - i\sin\tfrac{1}{2}Jt)|1_{+1}\rangle|2_0,2\rangle$$
$$+\tfrac{1}{20}(3\cos\tfrac{3}{2}Jt + 17\cos\tfrac{1}{2}Jt)|1_{+1}\rangle|1_0,3\rangle - \tfrac{\sqrt{3}}{10\sqrt{2}}(\cos\tfrac{3}{2}Jt - \cos\tfrac{1}{2}Jt)|1_{+1}\rangle|3_0,3\rangle]$$

$$|1_{+1}\rangle|3_0,3\rangle = e^{-iv_A t}[-\tfrac{1}{2\sqrt{2}\sqrt{5}}(i\sin\tfrac{3}{2}Jt - 3i\sin\tfrac{1}{2}Jt)|1_{+1}\rangle|0,0\rangle + \tfrac{\sqrt{3}}{2\sqrt{2}\sqrt{5}}(\cos\tfrac{3}{2}Jt - \cos\tfrac{1}{2}Jt)|1_{+1}\rangle|1_0,1\rangle$$
$$+\tfrac{1}{2\sqrt{2}\sqrt{5}}(i\sin\tfrac{3}{2}Jt - 3i\sin\tfrac{1}{2}Jt)|1_{+1}\rangle|0,2\rangle - \tfrac{1}{2\sqrt{5}}(i\sin\tfrac{3}{2}Jt + 3i\sin\tfrac{1}{2}Jt)|1_{+1}\rangle|2_0,2\rangle$$
$$-\tfrac{\sqrt{3}}{10\sqrt{2}}(\cos\tfrac{3}{2}Jt - \cos\tfrac{1}{2}Jt)|1_{+1}\rangle|1_0,3\rangle + \tfrac{1}{10}(\cos\tfrac{3}{2}Jt + 9\cos\tfrac{1}{2}Jt)|1_{+1}\rangle|3_0,3\rangle]$$

$$|0\rangle|1_{+1},1\rangle = e^{-iv_X t}[\cos\tfrac{1}{2}Jt|0\rangle|1_{+1},1\rangle - i\sin\tfrac{1}{2}Jt|1_0\rangle|1_{+1},1\rangle)]$$

$$|0\rangle|2_{+1},2\rangle = e^{-iv_X t}[\cos\tfrac{1}{2}Jt|0\rangle|2_{+1},2\rangle - i\sin\tfrac{1}{2}Jt|1_0\rangle|2_{+1},2\rangle)]$$

$$|0\rangle|1_{+1},3\rangle = e^{-iv_X t}[\cos\tfrac{1}{2}Jt|0\rangle|1_{+1},3\rangle - i\sin\tfrac{1}{2}Jt|1_0\rangle|1_{+1},3\rangle)]$$

$$|0\rangle|3_{+1},3\rangle = e^{-iv_x t}[\cos\tfrac{1}{2}Jt|0\rangle|3_{+1},3\rangle - i\sin\tfrac{1}{2}Jt|1_0\rangle|3_{+1},3\rangle]$$

$$|1_0\rangle|1_{+1},1\rangle = e^{-iv_x t}[-i\sin\tfrac{1}{2}Jt|0\rangle|1_{+1},1\rangle + \cos\tfrac{1}{2}Jt|1_0\rangle|1_{+1},1\rangle]$$

$$|1_0\rangle|2_{+1},2\rangle = e^{-iv_x t}[-i\sin\tfrac{1}{2}Jt|0\rangle|2_{+1},2\rangle + \cos\tfrac{1}{2}Jt|1_0\rangle|2_{+1},2\rangle]$$

$$|1_0\rangle|1_{+1},3\rangle = e^{-iv_x t}[-i\sin\tfrac{1}{2}Jt|0\rangle|1_{+1},3\rangle + \cos\tfrac{1}{2}Jt|1_0\rangle|1_{+1},3\rangle]$$

$$|1_0\rangle|3_{+1},3\rangle = e^{-iv_x t}[-i\sin\tfrac{1}{2}Jt|0\rangle|3_{+1},3\rangle + \cos\tfrac{1}{2}Jt|1_0\rangle|3_{+1},3\rangle]$$

$$|1_{+1}\rangle|2_{-2},2\rangle = e^{i(-v_\Delta+2v_x)t}[\cos\tfrac{1}{2}Jt|1_{+1}\rangle|2_{-2},2\rangle - i\sin\tfrac{1}{2}Jt|1_{+1}\rangle|3_{-2},3\rangle]$$

$$|1_{+1}\rangle|3_{-2},3\rangle = e^{i(-v_\Delta+2v_x)t}[-i\sin\tfrac{1}{2}Jt|1_{+1}\rangle|2_{-2},2\rangle + \cos\tfrac{1}{2}Jt|1_{+1}\rangle|3_{-2},3\rangle]$$

$$\begin{aligned}|1_{-1}\rangle|0,0\rangle = e^{iv_\Delta t}[&\tfrac{1}{4}(\cos\tfrac{3}{2}Jt + 3\cos\tfrac{1}{2}Jt)|1_{-1}\rangle|0,0\rangle + \tfrac{\sqrt{3}}{4}(i\sin\tfrac{3}{2}Jt + i\sin\tfrac{1}{2}Jt)|1_{-1}\rangle|1_0,1\rangle\\ &-\tfrac{1}{4}(\cos\tfrac{3}{2}Jt - \cos\tfrac{1}{2}Jt)|1_{-1}\rangle|0,2\rangle + \tfrac{1}{2\sqrt{2}}(\cos\tfrac{3}{2}Jt - \cos\tfrac{1}{2}Jt)|1_{-1}\rangle|2_0,2\rangle\\ &-\tfrac{\sqrt{3}}{4\sqrt{5}}(i\sin\tfrac{3}{2}Jt - 3i\sin\tfrac{1}{2}Jt)|1_{-1}\rangle|1_0,3\rangle + \tfrac{1}{2\sqrt{3}\sqrt{5}}(i\sin\tfrac{3}{2}Jt - 3i\sin\tfrac{1}{2}Jt)|1_{-1}\rangle|3_0,3\rangle]\end{aligned}$$

$$\begin{aligned}|1_{-1}\rangle|1_0,1\rangle = e^{iv_\Delta t}[&\tfrac{\sqrt{3}}{4}(i\sin\tfrac{3}{2}Jt + i\sin\tfrac{1}{2}Jt)|1_{-1}\rangle|0,0\rangle + \tfrac{1}{4}(3\cos\tfrac{3}{2}Jt + \cos\tfrac{1}{2}Jt)|1_{-1}\rangle|1_0,1\rangle\\ &-\tfrac{1}{4\sqrt{3}}(3i\sin\tfrac{3}{2}Jt - i\sin\tfrac{1}{2}Jt)|1_{-1}\rangle|0,2\rangle + \tfrac{1}{2\sqrt{6}}(3i\sin\tfrac{3}{2}Jt - i\sin\tfrac{1}{2}Jt)|1_{-1}\rangle|2_0,2\rangle\\ &-\tfrac{3}{4\sqrt{5}}(\cos\tfrac{3}{2}Jt - \cos\tfrac{1}{2}Jt)|1_{-1}\rangle|1_0,3\rangle + \tfrac{\sqrt{3}}{2\sqrt{2}\sqrt{5}}(\cos\tfrac{3}{2}Jt - \cos\tfrac{1}{2}Jt)|1_{-1}\rangle|3_0,3\rangle]\end{aligned}$$

$$\begin{aligned}|1_{-1}\rangle|0,2\rangle = e^{iv_\Delta t}[&-\tfrac{1}{4}(\cos\tfrac{3}{2}Jt - \cos\tfrac{1}{2}Jt)|1_{-1}\rangle|0,0\rangle - \tfrac{1}{4\sqrt{3}}(3i\sin\tfrac{3}{2}Jt - i\sin\tfrac{1}{2}Jt)|1_{-1}\rangle|1_0,1\rangle\\ &+\tfrac{1}{4}(\cos\tfrac{3}{2}Jt + 3\cos\tfrac{1}{2}Jt)|1_{-1}\rangle|0,2\rangle - \tfrac{1}{2\sqrt{2}}(\cos\tfrac{3}{2}Jt - \cos\tfrac{1}{2}Jt)|1_{-1}\rangle|2_0,2\rangle\\ &+\tfrac{1}{4\sqrt{3}\sqrt{5}}(3i\sin\tfrac{3}{2}Jt + 11i\sin\tfrac{1}{2}Jt)|1_{-1}\rangle|1_0,3\rangle - \tfrac{1}{2\sqrt{2}\sqrt{5}}(i\sin\tfrac{3}{2}Jt - 3i\sin\tfrac{1}{2}Jt)|1_{-1}\rangle|3_0,3\rangle]\end{aligned}$$

$$\begin{aligned}|1_{-1}\rangle|2_0,2\rangle = e^{iv_\Delta t}[&\tfrac{1}{2\sqrt{2}}(\cos\tfrac{3}{2}Jt - \cos\tfrac{1}{2}Jt)|1_{-1}\rangle|0,0\rangle + \tfrac{1}{2\sqrt{6}}(3i\sin\tfrac{3}{2}Jt - i\sin\tfrac{1}{2}Jt)|1_{-1}\rangle|1_0,1\rangle\\ &-\tfrac{1}{2\sqrt{2}}(\cos\tfrac{3}{2}Jt - \cos\tfrac{1}{2}Jt)|1_{-1}\rangle|0,2\rangle + \tfrac{1}{2}(\cos\tfrac{3}{2}Jt + \cos\tfrac{1}{2}Jt)|1_{-1}\rangle|2_0,2\rangle\\ &-\tfrac{1}{2\sqrt{5}\sqrt{6}}(3i\sin\tfrac{3}{2}Jt - i\sin\tfrac{1}{2}Jt)|1_{-1}\rangle|1_0,3\rangle + \tfrac{1}{2\sqrt{5}}(i\sin\tfrac{3}{2}Jt - 3i\sin\tfrac{1}{2}Jt)|1_{-1}\rangle|3_0,3\rangle]\end{aligned}$$

$$\begin{aligned}|1_{-1}\rangle|1_0,3\rangle = e^{iv_\Delta t}[&-\tfrac{\sqrt{3}}{4\sqrt{5}}(i\sin\tfrac{3}{2}Jt - 3i\sin\tfrac{1}{2}Jt)|1_{-1}\rangle|0,0\rangle - \tfrac{3}{4\sqrt{5}}(\cos\tfrac{3}{2}Jt - \cos\tfrac{1}{2}Jt)|1_{-1}\rangle|1_0,1\rangle\\ &+\tfrac{1}{4\sqrt{5}\sqrt{3}}(3i\sin\tfrac{3}{2}Jt + 11i\sin\tfrac{1}{2}Jt)|1_{-1}\rangle|0,2\rangle - \tfrac{1}{2\sqrt{5}\sqrt{6}}(3i\sin\tfrac{3}{2}Jt - i\sin\tfrac{1}{2}Jt)|1_{-1}\rangle|2_0,2\rangle\\ &+\tfrac{1}{20}(3\cos\tfrac{3}{2}Jt + 17\cos\tfrac{1}{2}Jt)|1_{-1}\rangle|1_0,3\rangle - \tfrac{\sqrt{3}}{10\sqrt{2}}(\cos\tfrac{3}{2}Jt - \cos\tfrac{1}{2}Jt)|1_{-1}\rangle|3_0,3\rangle]\end{aligned}$$

$$\begin{aligned}|1_{-1}\rangle|3_0,3\rangle = e^{iv_\Delta t}[&\tfrac{1}{2\sqrt{2}\sqrt{5}}(i\sin\tfrac{3}{2}Jt - 3i\sin\tfrac{1}{2}Jt)|1_{-1}\rangle|0,0\rangle + \tfrac{\sqrt{3}}{2\sqrt{2}\sqrt{5}}(\cos\tfrac{3}{2}Jt - \cos\tfrac{1}{2}Jt)|1_{-1}\rangle|1_0,1\rangle\\ &-\tfrac{1}{2\sqrt{2}\sqrt{5}}(i\sin\tfrac{3}{2}Jt - 3i\sin\tfrac{1}{2}Jt)|1_{-1}\rangle|0,2\rangle + \tfrac{1}{2\sqrt{5}}(i\sin\tfrac{3}{2}Jt + 3i\sin\tfrac{1}{2}Jt)|1_{-1}\rangle|2_0,2\rangle\\ &-\tfrac{\sqrt{3}}{10\sqrt{2}}(\cos\tfrac{3}{2}Jt - \cos\tfrac{1}{2}Jt)|1_{-1}\rangle|1_0,3\rangle + \tfrac{1}{10}(\cos\tfrac{3}{2}Jt + 9\cos\tfrac{1}{2}Jt)|1_{-1}\rangle|3_0,3\rangle]\end{aligned}$$

$$|0\rangle|1_{-1},1\rangle = e^{i\nu_x t}[\cos\tfrac{1}{2}Jt|0\rangle|1_{-1},1\rangle + i\sin\tfrac{1}{2}Jt|1_0\rangle|1_{-1},1\rangle]$$

$$|0\rangle|2_{-1},2\rangle = e^{i\nu_x t}[\cos\tfrac{1}{2}Jt|0\rangle|2_{-1},2\rangle + i\sin\tfrac{1}{2}Jt|1_0\rangle|2_{-1},2\rangle]$$

$$|0\rangle|1_{-1},3\rangle = e^{i\nu_x t}[\cos\tfrac{1}{2}Jt|0\rangle|1_{-1},3\rangle + i\sin\tfrac{1}{2}Jt|1_0\rangle|1_{-1},3\rangle]$$

$$|0\rangle|3_{-1},3\rangle = e^{i\nu_x t}[\cos\tfrac{1}{2}Jt|0\rangle|3_{-1},3\rangle + i\sin\tfrac{1}{2}Jt|1_0\rangle|3_{-1},3\rangle]$$

$$|1_0\rangle|1_{-1},1\rangle = e^{i\nu_x t}[i\sin\tfrac{1}{2}Jt|0\rangle|1_{-1},1\rangle + \cos\tfrac{1}{2}Jt|1_0\rangle|1_{-1},1\rangle]$$

$$|1_0\rangle|2_{-1},2\rangle = e^{i\nu_x t}[i\sin\tfrac{1}{2}Jt|0\rangle|2_{-1},2\rangle + \cos\tfrac{1}{2}Jt|1_0\rangle|2_{-1},2\rangle]$$

$$|1_0\rangle|1_{-1},3\rangle = e^{i\nu_x t}[i\sin\tfrac{1}{2}Jt|0\rangle|1_{-1},3\rangle + \cos\tfrac{1}{2}Jt|1_0\rangle|1_{-1},3\rangle]$$

$$|1_0\rangle|3_{-1},3\rangle = e^{i\nu_x t}[i\sin\tfrac{1}{2}Jt|0\rangle|3_{-1},3\rangle + \cos\tfrac{1}{2}Jt|1_0\rangle|3_{-1},3\rangle]$$

$$|1_{-1}\rangle|2_{+2},2\rangle = e^{i(\nu_A-2\nu_x)t}[\cos\tfrac{1}{2}Jt|1_{-1}\rangle|2_{+2},2\rangle + i\sin\tfrac{1}{2}Jt|1_{-1}\rangle|3_{+2},3\rangle]$$

$$|1_{-1}\rangle|3_{+2},3\rangle = e^{i(\nu_A-2\nu_x)t}[i\sin\tfrac{1}{2}Jt|1_{-1}\rangle|2_{+2},2\rangle + \cos\tfrac{1}{2}Jt|1_{-1}\rangle|3_{+2},3\rangle]$$

Zero Quantum Transitions

$$|1_{+1}\rangle|1_{-1},1\rangle = e^{i(-\nu_A+\nu_x)t}[\tfrac{1}{2}(\cos Jt + 1)|1_{+1}\rangle|1_{-1},1\rangle - \tfrac{1}{\sqrt{2}}(i\sin Jt)|1_{+1}\rangle|2_{-1},2\rangle$$
$$-\tfrac{1}{2\sqrt{5}}(\cos Jt - 1)|1_{+1}\rangle|1_{-1},3\rangle + \tfrac{1}{\sqrt{5}}(\cos Jt - 1)|1_{+1}\rangle|3_{-1},3\rangle]$$

$$|1_{+1}\rangle|2_{-1},2\rangle = e^{i(-\nu_A+\nu_x)t}[-\tfrac{1}{\sqrt{2}}(i\sin Jt)|1_{+1}\rangle|1_{-1},1\rangle + (\cos Jt)|1_{+1}\rangle|2_{-1},2\rangle$$
$$+\tfrac{1}{\sqrt{2}\sqrt{5}}(i\sin Jt)|1_{+1}\rangle|1_{-1},3\rangle - \tfrac{\sqrt{2}}{\sqrt{5}}(i\sin Jt)|1_{+1}\rangle|3_{-1},3\rangle]$$

$$|1_{+1}\rangle|1_{-1},3\rangle = e^{i(-\nu_A+\nu_x)t}[-\tfrac{1}{2\sqrt{5}}(\cos Jt - 1)|1_{+1}\rangle|1_{-1},1\rangle + \tfrac{1}{\sqrt{2}\sqrt{5}}(i\sin Jt)|1_{+1}\rangle|2_{-1},2\rangle$$
$$+\tfrac{1}{10}(9 + \cos Jt)|1_{+1}\rangle|1_{-1},3\rangle - \tfrac{1}{5}(\cos Jt - 1)|1_{+1}\rangle|3_{-1},3\rangle]$$

$$|1_{+1}\rangle|3_{-1},3\rangle = e^{i(-\nu_A+\nu_x)t}[\tfrac{1}{\sqrt{5}}(\cos Jt - 1)|1_{+1}\rangle|1_{-1},1\rangle - \tfrac{\sqrt{2}}{\sqrt{5}}(i\sin Jt)|1_{+1}\rangle|2_{-1},2\rangle$$
$$-\tfrac{1}{5}(\cos Jt - 1)|1_{+1}\rangle|1_{-1},3\rangle + \tfrac{1}{5}(2\cos Jt + 3)|1_{+1}\rangle|3_{-1},3\rangle]$$

$$|1_{-1}\rangle|1_{+1},1\rangle = e^{i(\nu_A-\nu_x)t}[\tfrac{1}{2}(\cos Jt + 1)|1_{-1}\rangle|1_{+1},1\rangle + \tfrac{1}{\sqrt{2}}(i\sin Jt)|1_{-1}\rangle|2_{+1},2\rangle$$
$$-\tfrac{1}{2\sqrt{5}}(\cos Jt - 1)|1_{-1}\rangle|1_{+1},3\rangle + \tfrac{1}{\sqrt{5}}(\cos Jt - 1)|1_{-1}\rangle|3_{+1},3\rangle]$$

$$|1_{-1}\rangle|2_{+1},2\rangle = e^{i(\nu_A-\nu_X)t}[\frac{1}{\sqrt{2}}(i\sin Jt)|1_{-1}\rangle|1_{+1},1\rangle + (\cos Jt)|1_{-1}\rangle|2_{+1},2\rangle$$
$$-\frac{1}{\sqrt{2}\sqrt{5}}(i\sin Jt)|1_{-1}\rangle|1_{+1},3\rangle + \frac{\sqrt{2}}{\sqrt{5}}(i\sin Jt)|1_{-1}\rangle|3_{+1},3\rangle]$$

$$|1_{-1}\rangle|1_{+1},3\rangle = e^{i(\nu_A-\nu_X)t}[-\frac{1}{2\sqrt{5}}(\cos Jt - 1)|1_{-1}\rangle|1_{+1},1\rangle - \frac{1}{\sqrt{2}\sqrt{5}}(i\sin Jt)|1_{-1}\rangle|2_{+1},2\rangle$$
$$+\frac{1}{10}(\cos Jt + 9)|1_{-1}\rangle|1_{+1},3\rangle - \frac{1}{5}(\cos Jt - 1)|1_{-1}\rangle|3_{+1},3\rangle]$$

$$|1_{-1}\rangle|3_{+1},3\rangle = e^{i(\nu_A-\nu_X)t}[\frac{1}{\sqrt{5}}(\cos Jt - 1)|1_{-1}\rangle|1_{+1},1\rangle + \frac{\sqrt{2}}{\sqrt{5}}(i\sin Jt)|1_{-1}\rangle|2_{+1},2\rangle$$
$$-\frac{1}{5}(\cos Jt - 1)|1_{-1}\rangle|1_{-1}\rangle|1_{+1},3\rangle + \frac{1}{5}(2\cos Jt + 3)|1_{-1}\rangle|3_{+1},3\rangle]$$

Double Quantum Transitions

$$|1_{+1}\rangle|1_{+1},1\rangle = e^{i(-\nu_A-\nu_X)t}[\frac{1}{2}(\cos Jt + 1)|1_{+1}\rangle|1_{+1},1\rangle - \frac{1}{\sqrt{2}}(i\sin Jt)|1_{+1}\rangle|2_{+1},2\rangle$$
$$-\frac{1}{2\sqrt{5}}(\cos Jt - 1)|1_{+1}\rangle|1_{+1},3\rangle + \frac{1}{\sqrt{5}}(\cos Jt - 1)|1_{+1}\rangle|3_{+1},3\rangle]$$

$$|1_{+1}\rangle|2_{+1},2\rangle = e^{i(-\nu_A-\nu_X)t}[-\frac{1}{\sqrt{2}}(i\sin Jt)|1_{+1}\rangle|1_{+1},1\rangle + (\cos Jt)|1_{+1}\rangle|2_{+1},2\rangle$$
$$+\frac{1}{\sqrt{2}\sqrt{5}}(i\sin Jt)|1_{+1}\rangle|1_{+1},3\rangle - \frac{\sqrt{2}}{\sqrt{5}}(i\sin Jt)|1_{+1}\rangle|3_{+1},3\rangle]$$

$$|1_{+1}\rangle|1_{+1},3\rangle = e^{i(-\nu_A-\nu_X)t}[-\frac{1}{2\sqrt{5}}(\cos Jt - 1)|1_{+1}\rangle|1_{+1},1\rangle + \frac{1}{\sqrt{2}\sqrt{5}}(i\sin Jt)|1_{+1}\rangle|2_{+1},2\rangle$$
$$+\frac{1}{10}(\cos Jt + 9)|1_{+1}\rangle|1_{+1},3\rangle - \frac{1}{5}(\cos Jt - 1)|1_{+1}\rangle|3_{+1},3\rangle]$$

$$|1_{+1}\rangle|3_{+1},3\rangle = e^{i(-\nu_A-\nu_X)t}[\frac{1}{\sqrt{5}}(\cos Jt - 1)|1_{+1}\rangle|1_{+1},1\rangle - \frac{\sqrt{2}}{\sqrt{5}}(i\sin Jt)|1_{+1}\rangle|2_{+1},2\rangle$$
$$-\frac{1}{5}(\cos Jt - 1)|1_{+1}\rangle|1_{+1},3\rangle + \frac{1}{5}(2\cos Jt + 3)|1_{+1}\rangle|3_{+1},3\rangle]$$

$$|0\rangle|2_{+2},2\rangle = e^{-i2\nu_X t}[\cos Jt|0\rangle|2_{+2},2\rangle - i\sin Jt|1_0\rangle|2_{+2},2\rangle]$$

$$|0\rangle|3_{+2},3\rangle = e^{-i2\nu_X t}[\cos Jt|0\rangle|3_{+2},3\rangle - i\sin Jt|1_0\rangle|3_{+2},3\rangle]$$

$$|1_0\rangle|2_{+2},2\rangle = e^{-i2\nu_X t}[-i\sin Jt|0\rangle|2_{+2},2\rangle + \cos Jt|1_0\rangle|2_{+2},2\rangle]$$

$$|1_0\rangle|3_{+2},3\rangle = e^{-i2\nu_X t}[-i\sin Jt|0\rangle|3_{+2},3\rangle + \cos Jt|1_0\rangle|3_{+2},3\rangle]$$

$$|1_{-1}\rangle|1_{-1},1\rangle = e^{i(\nu_A+\nu_X)t}[\frac{1}{2}(\cos Jt + 1)|1_{-1}\rangle|1_{-1},1\rangle + \frac{1}{\sqrt{2}}(i\sin Jt)|1_{-1}\rangle|2_{-1},2\rangle$$
$$-\frac{1}{2\sqrt{5}}(\cos Jt - 1)|1_{-1}\rangle|1_{-1},3\rangle + \frac{1}{\sqrt{5}}(\cos Jt - 1)|1_{-1}\rangle|3_{-1},3\rangle]$$

$$|1_{-1}\rangle|2_{-1},2\rangle = e^{i(\nu_A+\nu_X)t}[\frac{1}{\sqrt{2}}(i\sin Jt)|1_{-1}\rangle|1_{-1},1\rangle + (\cos Jt)|1_{-1}\rangle|2_{-1},2\rangle$$
$$-\frac{1}{\sqrt{2}\sqrt{5}}(i\sin Jt)|1_{-1}\rangle|1_{-1},3\rangle + \frac{\sqrt{2}}{\sqrt{5}}(i\sin Jt)|1_{-1}\rangle|3_{-1},3\rangle]$$

$$|1_{-1}\rangle|1_{-1},3\rangle = e^{i(\nu_A+\nu_X)t}[-\frac{1}{2\sqrt{5}}(\cos Jt - 1)|1_{-1}\rangle|1_{-1},1\rangle - \frac{1}{\sqrt{2}\sqrt{5}}(i\sin Jt)|1_{-1}\rangle|2_{-1},2\rangle$$
$$+\frac{1}{10}(\cos Jt + 9)|1_{-1}\rangle|1_{-1},3\rangle - \frac{1}{5}(\cos Jt - 1)|1_{-1}\rangle|3_{-1},3\rangle]$$

$$|1_{-1}\rangle|3_{-1},3\rangle = e^{i(\nu_A+\nu_X)t}[\frac{1}{\sqrt{5}}(\cos Jt - 1)|1_{-1}\rangle 1_{-1},1\rangle + \frac{\sqrt{2}}{\sqrt{5}}(i\sin Jt)|1_{-1}\rangle|2_{-1},2\rangle$$
$$-\frac{1}{5}(\cos Jt - 1)|1_{-1}\rangle|1_{-1},3\rangle + \frac{1}{5}(2\cos Jt + 3)|1_{-1}|3_{-1},3\rangle]$$

$$|0\rangle|2_{-2},2\rangle = e^{i2\nu_X t}[\cos Jt|0\rangle|2_{-2},2\rangle + i\sin Jt|1_0\rangle|2_{-2},2\rangle]$$

$$|0\rangle|3_{-2},3\rangle = e^{i2\nu_X t}[\cos Jt|0\rangle|3_{-2},3\rangle + i\sin Jt|1_0\rangle|3_{-2},3\rangle]$$

$$|1_0\rangle|2_{-2},2\rangle = e^{i2\nu_X t}[i\sin Jt|0\rangle|2_{-2},2\rangle + \cos Jt|1_0\rangle|2_{-2},2\rangle]$$

$$|1_0\rangle|3_{-2},3\rangle = e^{i2\nu_X t}[i\sin Jt|0\rangle|3_{-2},3\rangle + \cos Jt|1_0\rangle|3_{-2},3\rangle]$$

$$|1_{+1}\rangle|3_{-3},3\rangle = e^{i(-\nu_A+3\nu_X)t}|1_{+1}\rangle|3_{-3},3\rangle$$

$$|1_{-1}\rangle|3_{+3},3\rangle = e^{i(\nu_A-3\nu_X)t}|1_{-1}\rangle|3_{+3},3\rangle$$

Triple Quantum Transitions

$$|0\rangle|3_{+3},3\rangle = e^{-i3\nu_X t}[\cos\tfrac{3}{2}Jt|0\rangle|3_{+3},3\rangle - i\sin\tfrac{3}{2}Jt|1_0\rangle|3_{+3},3\rangle]$$

$$|1_0\rangle|3_{+3},3\rangle = e^{-i3\nu_X t}[-i\sin\tfrac{3}{2}Jt|0\rangle|3_{+3},3\rangle + \cos\tfrac{3}{2}Jt|1_0\rangle|3_{+3},3\rangle]$$

$$|1_{+1}\rangle|2_{+2},2\rangle = e^{i(-\nu_A-2\nu_X)t}[\cos\tfrac{1}{2}Jt|1_{+1}\rangle|2_{+2},2\rangle - i\sin\tfrac{1}{2}Jt|1_{+1}\rangle|3_{+2},3\rangle]$$

$$|1_{+1}\rangle|3_{+2},3\rangle = e^{i(-\nu_A-2\nu_X)t}[-i\sin\tfrac{1}{2}Jt|1_{+1}\rangle|2_{+2},2\rangle + \cos\tfrac{1}{2}Jt|1_{+1}\rangle|3_{+2},3\rangle]$$

$$|0\rangle|3_{-3},3\rangle = e^{i3\nu_X t}[\cos\tfrac{3}{2}Jt|0\rangle|3_{-3},3\rangle + i\sin\tfrac{3}{2}Jt|1_0\rangle|3_{-3},3\rangle]$$

$$|1_0\rangle|3_{-3},3\rangle = e^{i3\nu_X t}[i\sin\tfrac{3}{2}Jt|0\rangle|3_{-3},3\rangle + \cos\tfrac{3}{2}Jt|1_0\rangle|3_{-3},3\rangle]$$

$$|1_{-1}\rangle|2_{-2},2\rangle = e^{i(\nu_A+2\nu_X)t}[\cos\tfrac{1}{2}Jt|1_{-1}\rangle|2_{-2},2\rangle + i\sin\tfrac{1}{2}Jt|1_{-1}\rangle|3_{-2},3\rangle]$$

$$|1_{-1}\rangle|3_{-2},3\rangle = e^{i(\nu_A+2\nu_X)t}[i\sin\tfrac{1}{2}Jt|1_{-1}\rangle|2_{-2},2\rangle + \cos\tfrac{1}{2}Jt|1_{-1}\rangle|3_{-2},3\rangle]$$

Quad Quantum Transitions

$$|1_{+1}\rangle|3_{+3},3\rangle = e^{i(-\nu_A-3\nu_X)t}|1_{+1}\rangle|3_{+3},3\rangle$$

$$|1_{-1}\rangle|3_{-3},3\rangle = e^{i(\nu_A+3\nu_X)t}|1_{-1}\rangle|3_{-3},3\rangle$$

Appendix 4

Wigner Rotation Matrices for J = 0, 1, 2 and 3

$$d^0(\theta) = (0)$$

$$d^1(\theta) = \begin{pmatrix} \cos^2\left(\frac{\theta}{2}\right) & \frac{1}{\sqrt{2}}\sin\theta & \sin^2\left(\frac{\theta}{2}\right) \\ -\frac{1}{\sqrt{2}}\sin\theta & \cos\theta & \frac{1}{\sqrt{2}}\sin\theta \\ \sin^2\left(\frac{\theta}{2}\right) & -\frac{1}{\sqrt{2}}\sin\theta & \cos^2\left(\frac{\theta}{2}\right) \end{pmatrix}$$

$$d^2(\theta) = \begin{pmatrix} \cos^4\left(\frac{\theta}{2}\right) & -\frac{1}{2}\sin\theta(\cos\theta+1) & \sqrt{\frac{3}{8}}\sin^2\theta & \frac{1}{2}\sin\theta(\cos\theta-1) & \sin^4\left(\frac{\theta}{2}\right) \\ -\frac{1}{2}\sin\theta(\cos\theta-1) & \frac{1}{2}(2\cos\theta-1)(\cos\theta+1) & -\sqrt{\frac{3}{2}}\sin\theta\cos\theta & \frac{1}{2}(2\cos\theta+1)(1-\cos\theta) & \frac{1}{2}\sin\theta(\cos\theta-1) \\ \sqrt{\frac{3}{8}}\sin^2\theta & \sqrt{\frac{3}{2}}\sin\theta\cos\theta & \frac{1}{2}(3\cos^2\theta-1) & -\sqrt{\frac{3}{2}}\sin\theta\cos\theta & \sqrt{\frac{3}{8}}\sin^2\theta \\ -\frac{1}{2}\sin\theta(\cos\theta-1) & \frac{1}{2}(2\cos\theta+1)(1-\cos\theta) & \sqrt{\frac{3}{2}}\sin\theta\cos\theta & \frac{1}{2}(2\cos\theta-1)(\cos\theta+1) & -\frac{1}{2}\sin\theta(1+\cos\theta) \\ \sin^4\left(\frac{\theta}{2}\right) & -\frac{1}{2}\sin\theta(\cos\theta-1) & \sqrt{\frac{3}{8}}\sin^2\theta & \frac{1}{2}\sin\theta(1+\cos\theta) & \cos^4\left(\frac{\theta}{2}\right) \end{pmatrix}$$

$$d^3_{33}(\theta) = d^3_{-3-3}(\theta) = \cos^6\left(\frac{\theta}{2}\right)$$

$$d^3_{32}(\theta) = -d^3_{23}(\theta) = d^3_{-2-3}(\theta) = -d^3_{-3-2}(\theta) = -\sqrt{6}\cos^5\left(\frac{\theta}{2}\right)\sin\left(\frac{\theta}{2}\right)$$

$$d^3_{31}(\theta) = d^3_{13}(\theta) = d^3_{-1-3}(\theta) = d^3_{-3-1}(\theta) = \frac{\sqrt{15}}{8}\sin^2\theta(1+\cos\theta)$$

$$d^3_{30}(\theta) = -d^3_{03}(\theta) = d^3_{0-3}(\theta) = -d^3_{-30}(\theta) = -\frac{\sqrt{5}}{4}\sin^3\theta$$

$$d^3_{3-1}(\theta) = d^3_{-13}(\theta) = d^3_{1-3}(\theta) = d^3_{-31}(\theta) = \frac{\sqrt{15}}{8}\sin^2\theta(1-\cos\theta)$$

$$d^3_{3-2}(\theta) = -d^3_{-23}(\theta) = d^3_{2-3}(\theta) = -d^3_{-32}(\theta) = -\sqrt{6}\cos\left(\frac{\theta}{2}\right)\sin^5\left(\frac{\theta}{2}\right)$$

$$d^3_{3-3}(\theta) = d^3_{-33}(\theta) = \sin^6\left(\frac{\theta}{2}\right)$$

$$d^3_{22}(\theta) = d^3_{-2-2}(\theta) = \frac{1}{4}(1+\cos\theta)^2(3\cos\theta-2)$$

$$d^3_{21}(\theta) = -d^3_{12}(\theta) = d^3_{-1-2}(\theta) = -d^3_{-2-1}(\theta) = \frac{\sqrt{10}}{8}\sin\theta(1-3\cos\theta)(1+\cos\theta)$$

$$d^3_{20}(\theta) = d^3_{02}(\theta) = d^3_{0-2}(\theta) = d^3_{-20}(\theta) = \sqrt{\frac{15}{8}}\sin^2\theta\cos\theta$$

$$d^3_{2-1}(\theta) = -d^3_{-12}(\theta) = d^3_{1-2}(\theta) = -d^3_{-21}(\theta) = \frac{\sqrt{10}}{8}\sin\theta(1+3\cos\theta)(\cos\theta-1)$$

$$d^3_{2-2}(\theta) = d^3_{-22}(\theta) = \frac{1}{4}(1-\cos\theta)^2(3\cos\theta+2)$$

$$d^3_{11}(\theta) = d^3_{-1-1}(\theta) = \frac{1}{8}(1+\cos\theta)(15\cos^2\theta-10\cos\theta-1)$$

$$d^3_{10}(\theta) = -d^3_{01}(\theta) = d^3_{0-1}(\theta) = -d^3_{-10}(\theta) = \frac{\sqrt{3}}{4}\sin\theta(5\cos^2\theta-1)$$

$$d^3_{-11}(\theta) = d^3_{-11}(\theta) = \frac{1}{8}(1-\cos\theta)(15\cos^2\theta+10\cos\theta-1)$$

$$d^3_{00}(\theta) = \frac{1}{2}\cos\theta(5\cos^2\theta-3)$$

References

1. P.C. Taylor, J.F. Baugher and H.M. Kriz, *Chem. Rev.* **75**, 203, (1975).
2. Pople, J.A., Schneider, W.G. and Bernstein, H.J. *High-Resolution Nuclear Magnetic Resonance*, New York; McGraw-Hill Book Company, Inc., 1959.
3. Wuthrich, K. *NMR of Proteins and Nucleic Acids*, New York; John Wiley & Sons, Inc., 1986.
4. S. Aime and L. Milone, *Prog. Nucl. Magn. Reson. Spectrosc.* **11**, 183, (1977).
5. J.S. Hartman and B.L. Sherriff, *J. Phys. Chem.* **95**, 7575, (1991).
6. Y. Seo, M. Murakami, E. Suzuki, S. Kuki, K. Nagayama and H. Watari, *Biochemistry* **29**, 599, (1990).
7. E.M. Purcell, H.C. Torrey and R.V. Pound, *Phys. Rev.* **69**, 37, (1946).
8. F. Bloch, W.W. Hansen and M.E. Packard, *Phys. Rev.* **69**, 127, (1946).
9. W. Pauli, *Naturwiss.* **12**, 741, (1924).
10. D.A. Kleier and G. Binsch, *J. Magn. Reson.* **3**, 146, (1970).
11. K.G. Orrell and V. Sik, *Ann. Rep. NMR Spectrosc.* **19**, 79, (1987).
12. S. Forsen and R.A. Hoffman, *J. Chem. Phys.* **40**, 1189, (1964).
13. A.D. Bain, S.G. Hughes and G.K. Hamer, *J. Magn. Reson.* **96**, 613, (1992).
14. A.D. Bain, A.E. Hamielec and M. Mlekuz, *Macromolecules* (1991).(In Press)
15. M. Periyasamy and W.T. Ford, *Reactive Polymers* **3**, 351, (1985).
16. M. Karplus, *J. Chem. Phys.* **30**, 11, (1959).

17. M. Karplus, *J. Amer. Chem. Soc.* **85**, 2870, (1963).

18. M. Karplus, *J. Chem. Phys.* **33**, 1842, (1960).

19. G.M. Clore and A.M. Gronenborn, *Crit. Rev. Biochem. Mol. Biol.* **24**, 479 (1989).

20. K. Wuthrich, *Acc. Chem. Research* **22**, 36 (1989).

21. C. Griesinger, O.W. Sorensen and R.R. Ernst, *J. Magn. Reson.* **84**, 14 (1989).

22. G. Bodenhausen, R. Freeman, R. Niedermeyer and D.L. Turner, *J. Magn. Reson.* **26**, 133 (1977).

23. Martin, G.E. and Zektzer, A.S. *Two-dimensional NMR methods for establishing Molecular connectivity*, New York; VCH Publishers, 1988.

24. J. Jeener, *Ampere International Summer School, Yugoslavia* (1971).

25. D.M. Thomas, M.R. Bendall, D.T. Pegg, D.M. Doddrell and J. Field, *J. Magn. Reson.* **42**, 298, (1981).

26. A. Bax, *J. Magn. Reson.* **52**, 330, (1983).

27. W.P. Aue, E. Bartholdi and R.R. Ernst, *J. Chem. Phys.* **64**, 2229, (1976).

28. A.D. Bain, *J. Magn. Reson.* **77**, 125, (1988).

29. A.L. Waterhouse, I. Holden and J.E. Casida, *J. Chem. Soc. Perkin Trans. II* 1011, (1985).

30. K.G. Orrell, V. Sik and D. Stephenson, *Prog. Nucl. Magn. Reson. Spectrosc.* **22**, 141, (1990).

31. G.H. Weiss and J.A. Ferretti, *J. Magn. Reson.* **55**, 397, (1983).

32. A.A. Maudsley and R.R. Ernst, *Chem. Phys. Lett.* **50**, 368, (1977).

33. G. Bodenhausen and R. Freeman, *J. Magn. Reson.* **28**, 471, (1977).

34. A. Bax, *J. Magn. Reson.* **53**, 517, (1983).

35. J.R. Garbow, D.P. Weitekamp and A. Pines, *Chem. Phys. Lett.* **93**, 504, (1982).

36. H. Kessler, C. Griesinger, J. Zarbock and H.R. Loosli, *J. Magn. Reson.* **57**, 331, (1984).

37. A.D. Bain, *Prog. Nucl. Magn. Reson. Spectrosc.* **20**, 295, (1988).

38. A.D. Bain and J.S. Martin, *J. Magn. Reson.* **29**, 125, (1978).

39. A.D. Bain and J.S. Martin, *J. Magn. Reson.* **29**, 137, (1978).

40. A.D. Bain, *Chem. Phys. Lett.* **57**, 281, (1978).

41. A.D. Bain, *J. Magn. Reson.* **37**, 209, (1980).

42. A.D. Bain, *J. Magn. Reson.* **39**, 335, (1980).

43. Zare, R.N. *Angular Momentum: Understanding Spatial Aspects in Chemistry and Physics*, New York; John Wiley & Sons, 1988. pp. 1-349.

44. C.N. Banwell and H. Primas, *Mol. Phys.* **6**, 225, (1963).

45. Ernst, R.R., Bodenhausen, G. and Wokaun, A. *Principles of Nuclear Magnetic Resonance in One and Two Dimensions*, Oxford; Clarendon Press, 1987.

46. Rotenberg, M., Bivens, R., Metropolis, N. and Wooten, J.K.,Jr *The 3-j and 6-j Symbols*, Cambridge, MA; The Technology Press, MIT, 1959.

47. W.F. Reynolds, S. McLean, M. Perpick-Dumont and R.G. Enriquez, *Magn. Reson. Chem.* **27**, 162, (1989).

48. A.D. Bain, *J. Magn. Reson.* **56**, 418, (1984).

49. G. Bodenhausen, H. Kogler and R.R. Ernst, *J. Magn. Reson.* **58**, 370, (1984).

50. H.A. Buckmaster, *Can. J. Phys.* **42**, 386, (1964).

51. H.A. Buckmaster, *Can. J. Phys.* **44**, 2525, (1966).

52. Y.N. Chiu, *J. Chem. Phys.* **45**, 2969, (1966).

53. T. Allman and A.D. Bain, *J. Magn. Reson.* **68**, 533, (1986).

54. G. Bodenhausen and D.L. Turner, *J. Magn. Reson.* **41**, 200, (1980).

55. D.G. Hughes and G. Lindblom, *J. Magn. Reson.* **26**, 469, (1977).

56. G.V.T. Swapna, N. Sambasiva Rao and R. Ramachandran, *Magn. Reson. Chem.* **28**, 496, (1990).

57. J. Keeler, *J. Magn. Reson.* **56**, 463, (1984).

58. G. Bodenhausen, R. Freeman and D.L. Turner, *J. Magn. Reson.* **27**, 511, (1977).

59. K.E. Kover and Gy. Batta, *J. Magn. Reson.* **86**, 384, (1990).

60. G.V.T. Swapna, R. Ramachandran, N. Reddy and A.C. Kunwar, *J. Magn. Reson.* **88**, 135, (1990).

61. G.A. Morris and K.I. Smith, *Mol. Phys.* **61**, 467, (1987).

62. G.A. Morris and K.I. Smith, *J. Magn. Reson.* **65**, 506, (1985).

63. A.D. Bain, D.W. Hughes and H.N. Hunter, *Magn. Reson. Chem.* **26**, 1058, (1988).

64. W.F. Reynolds, S. McLean, M. Perpick-Dumont and R.G. Enriquez, *Magn. Reson. Chem.* **26**, 1068, (1988).

65. M. Perpick-Dumont, W.F. Reynolds and R.G. Enriquez, *Magn. Reson. Chem.* **26**, 358, (1988).

66. W.F. Reynolds, D.W. Hughes, M. Perpick-Dumont and R.G. Enriquez, *J. Magn. Reson.* **64**, 304, (1985).

67. H. Kessler, C. Griesinger and G. Zimmermann, *Magn. Reson. Chem.* **25**, 579,

(1987).

68. M. Rance, G. Wagner, O.W. Sorensen, K. Wuthrich and R.R. Ernst, *J. Magn. Reson.* **59**, 250, (1984).

69. A. Bax and R. Freeman, *J. Magn. Reson.* **44**, 542, (1981).

70. G. Bodenhausen, R. Freeman, G.A. Morris and D.L. Turner, *J. Magn. Reson.* **31**, 75, (1978).

71. G. Wider, R. Baumann, K. Nagayama, R.R. Ernst and K. Wuthrich, *J. Magn. Reson.* **42**, 73, (1981).

72. G.E. Martin, R.T. Gampe, J.J. Ford, M.R. Willcott, M. Morgan, A.L. Ternay, C.O. Okafor and K. Smith, *J. Heterocyclic Chem.* **20**, 1063, (1983).

73. T.T. Nakashima, B.K. John and R.E.D. McClung, *J. Magn. Reson.* **59**, 124, (1984).

74. A.D. Bain and J.S. Martin, *J. Magn. Reson.* **31**, 301, (1978).